The Electrical Activity of Saharan Dust as perceived from Surface Electric Field Observations

Vasiliki Daskalopoulou[1,2], Sotirios A. Mallios[2], Zbigniew Ulanowski[3,4], George Hloupis[5], Anna Gialitaki[2,6], Ioanna Tsikoudi[2,7], Konstantinos Tassis[8,9] and Vassilis Amiridis[2]

[1]Department of Physics, Faculty of Astrophysics and Space Physics, University of Crete, Heraklion GR-70013, Greece
[2]Institute for Astronomy, Astrophysics, Space Applications and Remote Sensing, National Observatory of Athens, Athens GR-15236, Greece
[3]Department of Earth and Environmental Sciences, University of Manchester, Manchester M13 9PL, UK
[4]British Antarctic Survey, NERC, Cambridge CB3 0ET, UK
[5]Department of Surveying and GeoInformatics Engineering, University of West Attica, Aegaleo Campus GR-12244, Greece
[6]Laboratory of Atmospheric Physics, Department of Physics, Aristotle University of Thessaloniki, Thessaloniki GR-54124, Greece
[7]Department of Environmental Physics and Meteorology, National and Kapodistrian University of Athens, Athens, Greece
[8]Department of Physics, and Institute for Theoretical and Computational Physics, University of Crete, Heraklion GR-70013, Greece
[9]Institute of Astrophysics, Foundation for Research and Technology-Hellas, Heraklion GR-71110, Greece

Correspondence to: Vassilis Amiridis (vamoir@noa.gr)

Abstract. We report on the electric field variations during Saharan dust advection over two atmospheric remote stations in Greece, using synergistic observations of the vertical atmospheric electric field strength (E_z) at ground level and the lidar-derived particle backscatter coefficient profiles. Both parameters were monitored for the first time with the simultaneous deployment of a ground-based field mill electrometer and a multi-wavelength polarization lidar. The field mill timeseries are processed to extract the diurnal variations of the Global Electric Circuit and remove fast field perturbations due to peak lightning activity. In order to identify the influence of the elevated dust layers on the ground E_z, we extract a Localized Reference Electric Field from the timeseries that reflects the local fair weather activity. Then, we compare it with the reconstructed daily average behaviour of the electric field and the Saharan dust layers' evolution, as depicted by the lidar. The observed enhancement of the vertical electric field (up to ~ 100 V/m), for detached pure dust layers, suggests the presence of in-layer electric charges. Although higher dust loads are expected to result in such a field enhancement, episodic cases that reduce the electric field are also observed (up to ~ 60 V/m). To quantitatively approach our results, we examine the dependency of E_z against theoretical assumptions for the distribution of separated charges within the electrified dust layer. Electrically neutral dust is approximated by atmospheric conductivity reduction, while charge separation areas within electrically active dust layers are approximated as finite extent cylinders. This physical approximation constitutes a more realistic description of the distribution of charges, as opposed to infinite extent geometries, and allows for analytical solutions of the electric field strength, so that the observed variations during the monitored dust outbreaks can be explained.

Keywords: Dust Electrification; Atmospheric Electric Field Measurements; Reference Electric Field; Charge Separation;

1 Introduction

The Global Electric Circuit (GEC) represents the electric current pathway in the Earth's atmosphere. The electric current that flows upwards from thunderstorms and electrified clouds into the Ionosphere, spreads out over the globe along magnetic field
40 lines to the opposite hemisphere, and returns to the surface of the Earth as the fair weather air-to-Earth current (Bering et al., 1998). The GEC is established by the conducting atmosphere sandwiched between the conductive Earth and the conductive Mesosphere/Ionosphere (Williams, 2009). Atmospheric electric parameters, such as the vertical Electric Field (E_z) and induced air-to-Earth current (I_c) through the GEC, greatly depend on ambient weather conditions and convective meteorological systems (Kourtidis et al., 2020) due to the re-distribution of charged or uncharged aerosols and terrestrial radioactive particles
45 in the Earth's atmosphere (Harrison and Ingram, 2005; Wright, 1933). Under fair weather conditions, which are defined according to international standards as those with cloudiness less than 0.2, wind speed less than 5 m/s and the absence of fog or precipitation (Chalmers, 1967; Harrison and Nicoll, 2018), the atmospheric electrical circulation is dominated by the potential difference between the global capacitor planes (about 250 kV, e.g., Rycroft et al., 2008), which in turn generates the fair weather electric field, and consequently the fair weather electric current in the presence of the conducting atmosphere. An
50 average current density of 2 pA/m^2 and a downward looking (by convention positive, e.g., Rakov and Uman, 2003, pp.8) electric field equal to a typical value of about 130 V/m are expected, respectively (Rycroft et al., 2008). The daily variation of the global thunderstorm activity modulates the electric field strength and the resulting diurnal variation is represented by the Carnegie curve (Harrison, 2013) .

Amongst the aerosols affecting the atmospheric electrical content (Whitby and Liu, 1966), mineral dust represents one of the
55 most significant contributors, along with volcanic ash (Harrison et al., 2010), due to its mineralogical composition that results in different electrical properties of the dust particles (Kamra, 1972) and its abundance in terms of dry mass (Tegen et al., 1997). During dust storms, dust devils and subsequent advection of elevated dust layers the electrical parameters can vary greatly from the values under fair weather conditions (Harrison et al., 2016; Renno and Kok, 2008; Zheng, 2013). It is well documented that over deserts the emission process of dust particles can generate large atmospheric electric fields (Esposito et al., 2016;
60 Renno and Kok, 2008; Zheng, 2013) that affect their flow dynamics (Kok and Renno, 2006). Charged dust occurrences are recorded via ground-based methods also in destinations further away from the source (Harrison et al., 2018; Katz et al., 2018; Silva et al., 2016; Yair et al., 2016; Yaniv et al., 2017), while balloon-borne observations (Kamra, 1972; Nicoll et al., 2011) indicate that space charge is indeed persistent within lofted dust layers during their transport to long distances. The exact mechanisms that would explain and sufficiently describe the long-range electrification of dust are not clear yet, and remain
65 under investigation. Major processes that are considered responsible for the electrification of dust particles include ion attachment (Tinsley and Zhou, 2006) and particle-to-surface or particle-to-particle collisions, i.e. triboelectrification (Kamra, 1972; Lacks and Shinbrot, 2019; Waitukaitis et al., 2014). Such processes are claimed to have large impact on desert dust transport and its influence in climate and ecosystems through the retention of larger dust particles in the atmosphere (van der

Does et al., 2018; Ryder et al., 2018), as well as to particle vertical orientation with impact on radiative transfer (Bailey et al., 2008; Mallios et al., 2021; Ulanowski et al., 2007).

Ground-based electric field measurements can be indicative of the electrical behaviour of elevated dust layers. These measurements can provide useful information if they are combined with other retrievals on aerosol profiling (e.g. lidar, ceilometer) (Nicoll et al., 2020). However, features of E-field timeseries, such as the enhancement of the near-ground electric field during dust outbreaks, are still unexplained in broad literature (Yaniv et al., 2016, 2017). Observations of enhanced or even reversed E-field at the height of the ground-based sensor, e.g. an electrostatic fieldmeter, are attributed by Ette (1971) and Freier (1960) to charge separation within electrically active dust. According to several laboratory studies (Duff and Lacks, 2008; Forward et al., 2009; Inculet et al., 2006; Waitukaitis et al., 2014), charge transfer processes lead to smaller particles being negatively charged while larger particles tend to be positively charged, therefore charge separation within lofted dust layers is also possible due to the expected size selective gravitational settling that could stratify the fine and coarse mode particles (Ulanowski et al., 2007). An observed reduction of the E-field in a mountainous area is attributed to the superposition of two dust layers in different heights with respect to the ground-based sensor (Katz et al., 2018). Moreover, layers that exhibit large particle densities lead to more particles competing for the same amount of ions (ion-particle competition, e.g. Gunn, 1954; Reiter, 1992), hence they act as a passive element within the atmospheric circulation and can reduce the near-ground electric field. A similar reduction of the electric field can be expected whenever, for any reason, the charge separation does not occur. As an example, one can think meteorological conditions that force the particles to move randomly, cancelling their vertical movement and, therefore, the charge separation. Nonetheless, systematic profiling measurements are needed so as to fully characterize the electrical properties of the dust particles aloft, with respect to the locally occurring meteorological conditions.

In this study, we focus on monitoring perturbations of the E-field near the ground caused by the transported dust layers, with special emphasis on slow E-field perturbations (with duration larger than 6 hours to exclude phenomena with small timescales or local effects of random origin), and we attempt to classify and comment on the electrical activity of the dust layers. As electrically active, we define the layers that exhibit charge separation and behave as electrostatic generators in the GEC, similarly to electrified shower clouds and thunderstorms (e.g. Mallios and Pasko, 2012). Conversely, electrically neutral are assumed to be the layers with no charge separation which, therefore, act as passive elements in the GEC, similarly to the non-electrified shower clouds (e.g. Baumgaertner et al., 2014). Four selected cases of Saharan dust plumes are examined, as captured over Finokalia and Antikythera atmospheric observatories by the same ground-based electrometer, as well as by the sophisticated Polly^{XT} lidar system. In Section 2, we provide an overview of the instrumentation and measurement techniques, and specify the methods used to parameterize the electrical behaviour of the dust layers. In Section 3, we present the modelled E-field behaviour which is used as a proof of concept for the explanation of the E-field diurnal variation (relative to the local reference field), presented in the results section along with the dynamic evolution of the dust episodes as revealed by the profiling information from the lidar. We further discuss whether the configuration of finite cylindrical charge accumulation

regions, previously suggested for the representation of charge distributions within thunderclouds (Krehbiel et al., 2008; Riousset et al., 2007), is capable of reproducing our experimental results. Finally, we present our conclusions in Section 6.

2 Data and methodology

105   We analyse four Saharan dust outbreaks recorded over two observational sites in Greece. The first atmospheric monitoring station is situated in the remote location of Finokalia (35.338° N, 25.670° E) on the north eastern coast of Crete, with the nearest large urban center being the city of Heraklion located 70 km to the west. The station is located at the top of a hill (252 m asl) facing the sea within a sector of 270° to 90° and the climatic characteristics are typical of the eastern Mediterranean basin exhibiting two distinctive seasons, the dry season (April to September) characterized by increased levels of pollution

110   and biomass burning and the wet season (October to April). Significant Saharan dust transport occurs when S/SW winds are prevalent during the intermediate season of March till June and may lead to ground concentrations exceeding 1 mg/m^3 (Solomos et al., 2018). Since there is no significant human activity occurring at a distance shorter than 15 km within the above sector, it makes it an appropriate location for monitoring dust layers advected directly from the Sahara. The second site is the PANhellenic GEophysical observatory (PANGEA) in the remote island of Antikythera (35.861° N, 23.310° E, 193 m asl). The

115   island covers an area of just 20.43 km^2, 38 km south-east of the larger island of Kythera and is devoid of human activity as its inhabitants are at most twenty people during early fall to mid-summer. The station location is ideal as the island is placed at a crossroad of air masses (Lelieveld et al., 2002), with NNE winds being prominent between August and February, while in spring and early summer western airflows that favor dust transport are observed. Moreover, the prevailing meteorological conditions on the island are again representative of the eastern Mediterranean with warm and dry days in summer in contrast

120   to winter, when the days are colder and wetter days are typical. The dust outbreaks recorded were on the 25th of July 2017 and March 16th 2018 on Finokalia, October 20th 2018 and June 23rd 2019 on Antikythera, selected due to the presence of elevated dust layers in the lidar profiles.

2.1 Aerosol monitoring and characterization

2.1.1 Lidar measurements

125   For the comprehensive characterization of dust particle optical properties, we exploit the profiling capabilities of the Polly[XT] Raman polarization lidar (Engelmann et al., 2016) of the National Observatory of Athens (NOA), as part of the European Aerosol Research Lidar Network (EARLINET). This multi-wavelength system is equipped with three elastic channels at 355, 532 and 1064 nm, two vibrational Raman channels at 387 and 607 nm, two channels for the detection of the cross-polarized backscattered signal at 355 and 532 nm, and one water vapour channel at 407 nm. The system employs two detectors, a near-

130   field and a far-field telescope provide reliable aerosol optical property profiles from close to the ground to the upper troposphere. The basic lidar quantities used for the monitoring and characterization of dust loads in our study, are the total attenuated backscatter coefficient (Mm^{-1}sr^{-1}) at 532 nm (calibrated range-corrected signal) to account for particle

concentrations and the Volume Linear Depolarization Ratio (VLDR, δ_v) at 532 nm. VLDR (%) is the ratio of the cross–polarized to the co-polarized backscattered signal (Freudenthaler et al., 2009), where cross- and co- are defined with respect to the plane of polarization of the emitted laser pulses. It encloses the influence of both atmospheric particles and molecules, with high δ_v values being indicative of irregular particles (i.e. atmospheric dust). However, for a comprehensive aerosol characterization, the particle backscatter coefficient (β) and Particle Linear Depolarization Ratio (PLDR, δ_p) are needed. PLDR (%) is derived from VLDR by correcting for molecular depolarization with atmospheric parameters extracted from radiosonde measurements (i.e. atmospheric pressure and temperature). In the selected case studies, we also present the δ_p and β profiles, as derived in the timeframe when each dust episode was fully developed. Typical δ_p values for Saharan dust are in the range of 25% to 35% at 532 nm, while large β values are representative of substantial particle concentrations (Haarig et al., 2017; Veselovskii et al., 2016, 2020).

2.1.2 Ancillary aerosol and trajectory information

The Aerosol Optical Depth (AOD) was monitored by a CIMEL sunphotometer, part of the Aerosol Robotic Network (AERONET - https://aeronet.gsfc.nasa.gov/), which was co-located with the lidar on both stations. For the cases examined here, the AOD varied from 0.221 to 0.366 at 500 nm. To characterize the air masses in regard to their origin we use the NOAA HYSPLIT back trajectory model, driven by GDAS meteorological data (https://www.ready.noaa.gov/HYSPLIT.php). The arrival heights for dust over the observational sites were selected in HYSPLIT according to the prevailing layering depicted by our lidar measurements (Fig. 1).

2.2 Electric Field measurements and data processing

2.2.1 Ground-based E-Field measurements

The JCI 131 Field mill (FM) electrometer (Chubb, 2014; Chubb, 2015) was installed in Finokalia from April 2017 until May 2018 (382 days) and then re-located to Antikythera, where the examined timeseries span from June 2018 to June 2019 (243 days) for continuous monitoring of the near-ground (on instrument mast height) vertical electric field. Field mills are robust instruments, mostly used for lightning warning applications providing, though, sufficient sensitivity for the detection of weaker electric fields. The instrument was mounted on a 3 m pole, and as far as possible from physical obstacles, buildings and any metallic objects that could create distortions to the electric field. However, on Finokalia the FM was on the edge of a hilly elevation which added a topography factor, not quantified in the specific research due to the lack of typical flat ground measurements in the area. On Antikythera, the mill installation location could be more carefully selected to avoid orography, obstacles and power grid lines. Instrument output range was set to the most sensitive scale (2.0 kV full scale) with a sensitivity of the order of 1 V/m for 1 Hz measurement frequency and the data were acquired from a 24-bit local data-logger. In order to interpret the field mill measurements, it is essential to compare the data with a reference field representative of local fair weather conditions. The methodology followed for this process is described in the paragraph below.

2.2.2 Derivation of the Localized Reference Electric Field

165 The classification of the vertical electric field behaviour under dust influenced conditions, as that of an enhanced, reduced or reversed E-field, necessitates comparison with the local long-term fair weather electric field. In order to represent solely the diurnal GEC influence at each observational site, away from electric generators perturbing the near ground E-field (e.g. Zhou and Tinsley, 2007), we construct a Localized Reference Electric Field (LREF) by exploiting only the timeseries inherent attributes and the measuring quantity itself, through the processing chain described below (Fig. 2). Various authors have

170 presented different methodologies for determining fair weather conditions (e.g. Anisimov et al., 2014). For the specific study, the selected constraints of fair weather are based on the classification of fair weather days as the less electrically disturbed days, also assumed by the Carnegie Institute researchers (Harrison, 2013). Although, local effects on the E-field at each site can be of random nature (wind gusts, lightning strikes, radon emission and turbulent flows due to orography), the selection of fair weather data can be based on noise reduction by subtracting values which are clearly dominated by local influences and

175 not directly addressing the meteorological criteria of fair weather (Harrison and Nicoll, 2018).

As such, the FM data are pre-processed by applying the appropriate scaling factor for the 3 m mounting mast of the electrometer (Chubb, 2015) and then days with no missing values due to either instrument malfunction, power outages or pc communication failures, are selected (Filter no.1). Under local fair weather conditions, the E-field, as measured here, is positive therefore imposing the second filtering step with a non-negativity constraint (Filter no. 2). When representing the E-field diurnal

180 variation by the Carnegie Curve, which is used consistently as a reference against locally measured atmospheric electricity parameters, the hourly variations of the field that shape the curve correspond to the 24, 12, 8, and 6-hour durations, as deduced from previous consistent observations of the Carnegie vessel (Harrison, 2013). The present study attempts to derive the local harmonic fit in the form of the LREF, based on the Carnegie curve morphology, and assuming that this trend should be followed by the reference field as well. Consequently, the averaged 1s data to 1-minute data (datalogger configuration) are shifted to

185 the frequency domain through a Fast Fourier Transform (FFT) representation so as to evaluate the relative contributions of the first five principal harmonics to the diurnal cycle of the electric field (hourly variations including daily mean), which are depicted in the following signal equation for $S(t)$ (1). We note, that days with missing data are removed, because the uneven temporal distribution of the measurements modifies the time window for the FFT algorithm, and therefore, modifies the timeseries spectrum.

$$S(t) = A_0 + A_1 \cos(2\pi f_1 + \varphi_1) + A_2 \cos(2\pi f_2 + \varphi_2) + A_3 \cos(2\pi f_3 + \varphi_3)$$
$$+ A_4 \cos(2\pi f_4 + \varphi_4) \tag{1}$$

190

where S is the electric field at time t in hrs (UTC), A_i for $i = 0, ..4$ where A_0 represents the mean value (constant, zeroth harmonic) and A_1 to A_4 (first to fourth harmonic) represent the amplitudes of the 24, 12, 8, and 6-hour variations, $f_i = i\frac{t}{24}360°$ is the frequency of each harmonic, where $f_0 = 0$ and φ_i are the respective phases in degrees, with $\varphi_0 = 0$ (Harrison, 2013). Based on the form of the Carnegie curve, and assuming that this trend should be followed by the reference field as well,

195 we find empirically that the ratio between the zeroth harmonic and the first harmonic is around two. Therefore, the E_z values

for which the amplitude A_0 is larger than two times the amplitude A_1 are kept (Filter no. 3). The same filter is applied to the other harmonics as well (A_0 is larger than two times the A_i), making sure that no fast-transient contribution is kept.

Lastly, since the amplitude of each harmonic is expected to be constant for all days (as the amplitudes in the Carnegie curve do), we impose the Chauvenet criterion on each of the filtered five harmonics amplitude, so as to detect outliers. The criterion is imposed once with the use of the relation below:

$$N \, erfc\left(\frac{d^j}{\sqrt{2}s}\right) < \frac{1}{2} \tag{2}$$

for a deviation of:

$$d^j = \left|A_i{}^j - \bar{A}_i\right|$$

where $i = 0,..4$ refers to the ith harmonic, $j = 0,..N$ day number and N the total number of days, for

$$\bar{A}_i = \frac{1}{N}\sum_{j=1}^{N} A_i{}^j$$

where A_{ij} is the ith harmonic amplitude per day and summated over j gives $\bar{A}_i$ as the mean amplitude of each harmonic. Lastly, erfc(x) is the complementary error function, defined as:

$$erfc(x) = 1 - erf(x) = 1 - \frac{2}{\sqrt{\pi}}\int_0^x e^{-t^2}dt$$

Also s is the unbiased sample variance and is defined as:

$$s^2 = \frac{\sum_{j=1}^{N}\left(A_i{}^j - \bar{A}_i\right)^2}{N-1}$$

After the Chauvenet criterion is met, 152 total undisturbed weather days are detected for Finokalia and 109 days for Antikythera. From this reduced dataset, we reconstruct the LREF by keeping the mean values of the first three harmonics and calculate the respective standard errors as $\pm 2SE$ from the reconstructed signal.

2.2.3 E-field measurement comparison

In order to compare LREF with the daily variation of the electric field during the dust events, these field mill measurements are also shifted to the frequency domain through an FFT. Again, the first five harmonics are retained and from the specific dataset, a smoothed slow varying field is reconstructed (otherwise referred to as reconstructed mean for the remainder of this paper) from the set of mean amplitudes and phases of the first three harmonics. This filtered field retains the main characteristics of the local reference field., since fast transient events which are less than 6 hrs in duration are removed. Therefore, the LREF and reconstructed mean field signals that are compared have the same spectral information. Moreover, to compare the E-field timeseries with the lidar retrievals, all the field mill data are further averaged to 5 mins.

2.3 Mathematical formalism for the modelling of the ground E-field

Ideally, under strict fair weather conditions, complete lack of aerosol particles in the atmospheric circulation is expected, since it guarantees that the only mechanism of atmospheric ions loss is the ion-ion recombination. As the concentration of aerosols increases, additional loss can be due to ions attaching to the particles, which leads to a perturbation of the ion density from fair weather values. In actual conditions, aerosols always exist, but under fair weather conditions their concentrations are small enough to not significantly affect the ionic content of the atmosphere. Therefore, for the modelling purposes of fair weather conditions, aerosol concentrations can be neglected. In the steady state of such an atmosphere, the divergence of the total current is zero $\vec{\nabla}\vec{J}_{tot} = 0$, as a direct consequence of the continuity equation and hence the conduction current remains constant with altitude. From Ohm's law, we can relate the conduction current with the vertical component of the electric field (Fig. 3a), as:

$$J_z = \sigma E_z \tag{3}$$

where σ is the atmospheric conductivity and assume a smooth conductivity profile along the altitude z, as:

$$\sigma = \sigma_0 \, exp\left(\frac{z}{l}\right) \tag{4}$$

for σ_0 and l the constants that represent the near ground atmospheric conductivity and the atmospheric scale height respectively. The given mathematical formalism of the atmospheric conductivity is adopted also by Ilin et al. (2020). The authors demonstrated that such a profile adequately describes the main aspects of the real conductivity distribution, and can be seen as a global mean conductivity profile.

We, then, express the conduction current at ground level, J_{z_0}, as a function of the columnar resistance R_c and the potential difference $\Delta V = V_{ion} - V_0$, where V_{ion} is the ionospheric potential at the altitude H, and V_0 is the potential at the Earth's surface which is considered a good conductor due to soil particles that are usually covered by a thin, conducting film of water (Kanagy and Mann, 1994), hence V_0 is set equal to zero. Therefore:

$$J_{z_0} = \frac{V_{ion}}{R_c} \tag{5}$$

The columnar resistance can be calculated from the conductivity profile of equation (4) (Rycroft et al., 2008), hence:

$$R_c = \int_0^H \frac{dz}{\sigma} = \frac{l}{\sigma_0}\left(1 - exp\left(-\frac{H}{l}\right)\right) \tag{6}$$

By combining equations (3), (5) and (6), the fair weather electric field at ground level is of the form (Gringel et al. 1986):

$$E_{z_0} = \frac{V_{ion}}{\sigma_0 R_c} = \frac{V_{ion}}{l\left(1 - exp\left(-\frac{H}{l}\right)\right)} \tag{7}$$

which depends solely on the scale height l and the ionospheric potential V_{ion}.

However, the presence of aerosols in the atmosphere and consequently dust particles, affects atmospheric conductivity (Harrison, 2003; Siingh et al., 2007; Tinsley and Zhou, 2006; Zhou and Tinsley, 2007). Aerosols tend to scavenge atmospheric ions due to electrostatic interactions and ion thermal diffusion, leading to a reduction of the atmospheric ion density, and

consequently of the atmospheric electrical conductivity. The process of ion attachment to aerosols has been exhaustively investigated in the past literature. A review paper by Long and Yao (2010) contains a summary of all models and theories regarding the aerosol charging by ions. The case of a steady state atmospheric desert dust layer that does not exhibit charge stratification is examined below. The layer acts as a passive electrical element (resistor), and reduces the fair weather atmospheric conductivity due to the ion attachment to dust particles, by a reduction varying factor n. Fig. 3b, represents the above layer configuration, where the new conductivity profile within the layer will be:

$$\sigma' = \frac{\sigma_0}{n} exp\left(\frac{z}{l}\right) \tag{8}$$

The electric field at ground due to the dust layer, $E_{z_0,layer}$, is given by:

$$E_{z_0,layer} = \frac{V_{ion}}{\sigma_0 R_c'} \tag{9}$$

with the columnar resistance being:

$$R_c' = \int_0^{z_1} \frac{dz}{\sigma} + \int_{z_1}^{z_1} \frac{dz}{\sigma'} + \int_{z_1}^{H} \frac{dz}{\sigma}, \qquad z \neq z_{1,2} \quad \Rightarrow$$

$$R_c' = \frac{l}{\sigma_0}\left[1 + (n-1)exp\left(-\frac{z_c - d/2}{l}\right)\left(1 - exp\left(-\frac{d}{l}\right)\right) - exp\left(-\frac{H}{l}\right)\right] \tag{10}$$

And (9) gives through (10):

$$E_{z_0,layer} = \frac{V_{ion}}{l\left[1 + (n-1)exp\left(-\frac{z_c - d/2}{l}\right)\left(1 - exp\left(-\frac{d}{l}\right)\right) - exp\left(-\frac{H}{l}\right)\right]} \tag{11}$$

where $z_{1,2}$ are the layer bottom/top heights, z_c is the mean layer central height, d is the mean layer depth and R, as presented in Fig. 3b, is the layer horizontal extent (radius) which is assumed to be at least ten times larger than its vertical extent ($R \geq 10d$). Therefore, it is clear that $E_{z_0,layer}$ depends on the scale height parameter l, the reduction parameter n, the layer central height z_c and the layer depth $d = z_2 - z_1$. A further investigation of the E-field dependence on the various parameters listed above can be found in the Appendix A.

On a next step, we parameterize an electrically active dust layer to calculate its impact on the surface E-field. Specifically, we construct a simplistic model for the atmospheric column (1D), based on the hypothesis that the charge accumulation areas within the dust layer can be approximated by charged cylinders of a total charge density $\pm\rho$ (Fig. 3c). For the cylinder, we assume that its horizontal extent, as represented by the cylinder radius, is at least 10 times larger than the vertical extent (large cloud approximation), to ensure that the field lines are vertical with only weak radial dependence directly below the center of the layer (e.g. Riousset et al., 2007). The electric field of such an idealized finite extent charged layer is dependent on the distance from the layer. Departures from this behaviour occur near layer edges and distances comparable to the layer extent. Moreover, the hypothesis of the presence of image charges is also applied due to the ground being a good conductor, ensuring that the calculated electric potentials are solutions to the Poisson equation.

The formulation for such an electrically active layer consists of a superposition of the electrically neutral dust layer case with the monopole charged cylinder case, constrained for zero ground and zero ionospheric potentials. The derivation of the ground electric field due to the presence of a total charge density of ρ is given below. We calculate the potential at point A (central lower point of the charged cylinder), as specified in Fig. 3c, which is given as the sum of the potential from Q and the potential from its image Q_{img}, where $Q_{img} = -Q$:

$$V_A = V_Q + V_{Q_{img}} \tag{12}$$

The solution for the potential at the central axis of a solid charged cylinder with total charge density ρ_1, is given by (e.g. Griffiths Instructor's Solution Manual for Introduction to Electrodynamics, 4th Edition, 2013):

$$V_Q = \frac{\rho_1}{4\varepsilon_0}\left\{ d_1\sqrt{R_1^2 + d_1^2} + R_1^2 \ln\left[\frac{d_1 + \sqrt{R_1^2 + d_1^2}}{R_1}\right] - d_1^2 \right\}, \qquad for\ R_1 \geq 10d_1 \tag{13}$$

where ε_0 is the permittivity of vacuum, R_1 the charge region horizontal extent presented by the cylinder radius, $d_1 = z_2' - z_1'$ the cylinder depth (charge region vertical extent) and ρ_1 is the total charge density. Correspondingly, the potential at point A due to the image charge is calculated as:

$$V_{Q_{img}} = \frac{-\rho_1}{4\varepsilon_0}\left\{ 2z_{c_1}\sqrt{R_1^2 + (2z_{c_1})^2} - (2z_{c_1} - d_1)\sqrt{R_1^2 + (2z_{c_1} - d_1)^2} \right.$$

$$\left. + R_1^2 \ln\left[\frac{2z_{c_1} + \sqrt{R_1^2 + (2z_{c_1})^2}}{(2z_{c_1} - d_1) + \sqrt{R_1^2 + (2z_{c_1} - d_1)^2}}\right] - 2d_1\left(2z_{c_1} - \frac{d_1}{2}\right) \right\} \tag{14}$$

The new columnar resistance up to the height of point A will be:

$$R_{c_1} = \int_0^{z_1}\frac{dz}{\sigma} + \int_{z_1}^{z_1'}\frac{dz}{\sigma'} \Rightarrow \tag{}$$

$$R_{c_1} = \frac{l}{\sigma_0}\left[1 - exp\left(-\frac{z_c - d/2}{l}\right)\right] + \frac{nl}{\sigma_0}\left[exp\left(-\frac{z_c - d/2}{l}\right) - exp\left(-\frac{z_{c_1} - d_1/2}{l}\right)\right] \tag{15}$$

And again, from Ohm's law and equation (15), we get the electric field at ground level for the case of a charged cylindrical monopole as:

$$E_{z_0,Q} = \frac{V_A}{l\left[1 - exp\left(-\frac{z_c - d/2}{l}\right)\right] + nl\left[exp\left(-\frac{z_c - d/2}{l}\right) - exp\left(-\frac{z_{c_1} - d_1/2}{l}\right)\right]} \tag{16}$$

with $E_{z_0,Q}$ being dependent on the scale height l, the conductivity reduction factor n, the central layer height z_c and the charged area central height z_{c_1}.

285 In the case of multiple stratified charged areas within the layer, the electric field at ground level is a superposition of the contribution to the field from each charge and its image (E_{z_0, Q_i}), along with the non-stratified dust layer's contribution attributed to the imposed conductivity reduction ($E_{z_0, layer}$), hence:

$$E_{z_0, multipole} = \sum E_{z_0, Q_i} + E_{z_0, layer} \Rightarrow$$

$$E_{z_0, dipole} = E_{z_0, \text{lower cylinder}} + E_{z_0, \text{upper cylinder}} + E_{z_0, layer}$$

(17)

3 Model outputs

As a result of the mathematical formalism described in Section 2.3, we present the 1D model outputs and restrictions under
290 which the various behaviors of the near-ground E-field strength can be exhibited in comparison to the calculated fair weather E-field. Following this formulation, the dust layer that exhibits charge separation is approximated with a dipole of oppositely charged cylinders. The influence of small charge imbalances, less than 10%, in the bipolar case, which could quantitatively explain the enhancement or reduction in the E-field is also investigated. If multiple charge accumulation regions are suspected within the dust layer (Zhang and Zhou, 2020), the problem can be still represented by the model output through a superposition
295 of several cylindrical monopoles with different charge densities, polarities and separation distances.

3.1 E-field below Fair weather field

In this section, we describe the possible cases under which lofted dust layers can reduce the near-ground E-field strength below the reference electric field values, and we investigate whether electrified dust layers can reproduce such a behaviour. $E_{z_0, layer}$ dependency on the various atmospheric parameters points to atmospheric conductivity as the dominant factor that affects the
300 E-field (see Appendix A). Therefore, we expect that if the dust layer is electrically neutral and acts as a passive element by reducing the atmospheric conductivity, it will greatly affect the field by forcing it below the local reference values.

Since there is little data on vertical profiling of the dust layer electrical properties, we use previous measurements of the electric field variation with altitude, which indicated a charge density of $\rho = \pm 25$ pC/m^3 within a transported Saharan dust layer away from the emission source (Nicoll et al., 2011). From the specific value, the total charge Q is estimated for the different model
305 cylinder extents. Gringel and Muhleisen (1978) measured a reduction of the electrical conductivity, compared to the fair weather values, by a factor of four within an elevated dust layer and we, therefore, adopt a reduction factor of $n = 4$ in the present study (see also Appendix A). For E_{z_0}, $E_{z_0, layer}$ and $E_{z_0, Q}$, estimations, the scale height is fixed to a globally average value of $l = 6$ km (Kalinin et al., 2014; Stolzenburg and Marshall, 2008), the ionospheric potential is fixed at $V_{ion} = 250$ kV and the ionospheric height is at $H = 70$ km. The mean central height of the dust layer and mean layer depth are both set equal
310 to 3 km ($z_c = d = 3$ km), since this height represents the average value for the four dust cases according to the lidar PLDR profiles (Table 1).

3.1.1 Balanced/Imbalanced dipole field below Fair weather field

We consider the case of two oppositely charged cylinders with similar geometries as in Fig. 3c, assuming they are within a dust layer with a mean height of 3 km and a mean depth of 3 km. The lower cylinder central height z_{c_1} starts at 2.95 km and decreases, the upper cylinder central height z_{c_2} starts also at 2.95 km for zero separation distance (at this limit, it represents electrically neutral dust that lacks internal E-field generation due to the absence of charge separation) and increases within the dust layer boundaries (varying separation distance), while their depth is fixed at 100 m, in order to be of finite vertical extend but quite thin. The separation distance between the two cylinders is defined as the difference between their central heights and the ground E-field is a superposition of the electric field of the upper and lower cylinders. We assume the bottom cylinder to be positively charged with density $+\rho$ and the upper one to be negatively charged with $-\rho$ (Fig. 4a), in order to simulate gravitational settling conditions for larger and, most probably, positively charged dust particles (Forward et al., 2009; Waitukaitis et al., 2014). From equations (12) to (17), the field is analytically calculated directly on the axis of the charged cylinders and plotted against the cylinder radius R for separation distances up to 800 m. As seen in Fig. 4, the resulting electric field values on ground level are consistently below the fair weather constant value. When the dipole separation distance increases, the vertical electric field at ground level increases, but when kept relatively small, the E-field increases but not sufficiently to overcome the fair weather field (Fig. 4). This happens due to the fact that as the upper charged layer moves to higher altitudes, the resistance between the layer and the ground increases, therefore the conduction current at the ground decreases. The conduction current due to the upper charged layer becomes weaker than the conduction current due to the lower charged layer, which moves towards the ground. Since the conductivity at the ground is undisturbed by the layer and equal to the fair weather value, the ground electric field due to the upper layer decreases as the layer moves up, while the field due to the lower layer increases as the layer approaches the ground, leading to an increasing value of the total electric field with the increasing separation distance. For large radii, although the infinite plates configuration is asymptotically approached ($E_{z_0,dipole} \to 0$), there is a nearly-constant residual field for the finite cylindrical geometry of the charged regions. Since the charged cylinders are placed in a conducting medium above a perfect conductor, the electric field at the ground will not be zero even if the cylinders have infinite extent. Due to the conductivity distribution, there is an uneven contribution of the electric fields of each cylinder and, therefore, the E-field is expected to converge to this non-zero value (Fig. 4).

If the dipole charge density is not uniformly distributed to both cylinders, resulting in a charge imbalance within the layer, the electric field will be more sensitive to separation distance changes (Fig. 4b). Such imbalance could be the result of (a) dust charging at the source, prior to any charge separation that may occur (Ette, 1971; Kamra, 1972), (b) charging due to atmospheric current, or (c) charge loss through dry deposition in the Planetary Boundary Layer (PBL). In Fig. 5, the ground electric field dependence on the separation distance and cylinder radius is depicted, for a charge density difference of $\Delta\rho = 2$ pC/m^3 between the two charged cylindrical areas, with the upper one being less charged. This leads to a larger increase of the E-field than in the balanced dipole case (Fig. 4a), as the effect of the upper cylinder not only decreases as it moves to higher altitudes, but it is also reduced due to the reduction of the total charge density which influences proportionally the electric

345 field. Note that even a small imbalance can highly increase the external field. Nevertheless, for relatively small separation distances the resulting field values fall below the fair weather value.

3.2 E-field above Fair weather field

We examine the physical arrangement within the dust layer that can provide an enhancement to the electric field above the fair weather values and subsequently above the LREF.

350 3.2.1 Balanced/Imbalanced dipole field above Fair weather field

For the same charged region geometries as discussed previously, larger separation distances are imposed for the balanced dipole case (Fig. 5a), but strictly remain within the base dust layer mean dimensions. Fig. 5 shows that as the separation distance between the oppositely charged layers increases, an enhancement of the E-field above the local reference values occurs. This enhancement becomes more prominent as the layers grow further apart within the dust plume and the contribution

355 from the lower layer is significantly larger than the upper layer. The above dependence of the ground E-field on the separation distance is not expected in the case of charged infinite plates, as discussed in Section 3.1.1. Again, for a charge imbalance of 8% between the two cylinders and for larger separation distances, the E-field is significantly enhanced and exceeds the local fair weather values (Fig. 5b). The term large or small separation distance depends on the conductivity distribution and more specifically on the conductivity scale height, as can be seen in equations (11) and (16). This increase becomes more prominent

360 as the separation distance increases and the lower positive cylinder moves closer to the sensor location.

4 Experimental Results

The near ground electric field measurements with co-located lidar observations are presented for our case studies of elevated Saharan dust layers, over the two atmospheric remote sensing stations. The transient dust events recorded by Polly[XT] were, simultaneously, electrically monitored throughout the day with the field mill. According to the effect over the E-field

365 timeseries, the dust outbreaks examined are separated into two classes, the ones that effectuate an enhancement to the ground electric field and those inducing a reduction with respect to the local reference field. Through these observations, we attempt to provide evidence of electrically active dust only by ground-based methods, supported by the model configuration described in the previous sections.

4.1 Layer characterization through Polly[XT]

370 The July 2017 and March 2018 dust events, in Finokalia, are characterized by large concentrations of airborne dust particles from the middle of the day onwards, followed by dust settling towards the ground after 21:00 (UTC), as indicated by the time-height plots of the total attenuated backscatter coefficient (Fig. 6 and Fig. 8). Larger particle concentrations are shown in red tones, with the β and δ_p (black lines) superimposed to the respective attenuated backscatter coefficient (top panel) and δ_v (lower

panel) quick-looks. For the first case study, settling of dust particles below 2 km, inside the Marine Boundary Layer (MABL) is revealed from the increased VLDR values (>10%; see Fig. 6), while for the second case study dust downward mixing inside the MABL is less prominent (see Fig. 8). As observed in Fig. 8, the elevated layer (small dust concentration is present near the surface) reached Finokalia in March 16th 2018, at early noon. The layer was directly transported from Sahara and reached the station in less than 48 hours, as indicated by the backward trajectories analysis (Fig. 1c). Maximum β value on July 25th reaches at 5 (Mm^{-1}sr^{-1}) inside the dust layer, while on March 16th, β values reach at 15 (Mm^{-1}sr^{-1}) at the top of the layer, indicating higher aerosol concentrations in the second case. The δ_p values vary from 20% - 25% for the first case and from 20% - 30% for the second case, pointing to pure dust areas.

The October 20th 2018 Antikythera layer (Fig. 7), exhibits lower dust particle concentrations (< 5 Mm^{-1}sr^{-1}) close to the ground up to 6 km in altitude, mostly mixed with marine aerosols below 2 km (Fig. 1b and Fig. 7). It is also observed that the near-ground dust concentration is very low, with the thin layer at 500 m being a mixture of dust particles and particles of marine origin with VLDR values around 15%. The June 23rd 2019 dust outbreak consists primarily of high elevated dust concentrations (Fig. 1d), after mid-day, with dust PLDR values reaching up to 30% in the height range of 3 - 5 km, representative of pure dust (Fig. 9). The dust plume was transported again directly from Sahara to Antikythera within 48 hours (Fig. 1d) and very low concentrations of dust particles are also present within the MABL.

4.2 Local mean E-field behaviour

Considering the electrical properties of the layers detected in Finokalia (Fig. 6 and Fig. 8), the LREF and the reconstructed mean electric field are depicted, with the local diurnal variation resembling the Carnegie curve. The E_z values vary between a total minimum at ~ 05:00 (UTC) and the maximum at ~ 13:00 (UTC) with a mean value of ~ 173 V/m. An increase of the electric field is observed at about 22:00 (UTC) resulting in a double peak variations curve (Yaniv et al., 2016). The reconstructed mean E-field is close to the expected fair weather value and the slight difference can be attributed to local meteorological factors, atmospheric boundary layer characteristics (Anisimov et al., 2017) and the station's coastal location. Complementarily, E_z diurnal variation in the station of Antikythera exhibits a minimum in early morning hours at ~ 23:00 (UTC) and a single maximum on early afternoon at ~ 19:00 (UTC) (Fig. 7 and Fig. 9), with a mean value of ~ 102 V/m. Since the timeseries in Antikythera are restricted to one year, the mean E-field value is statistically biased, therefore it is lower than the expected fair weather value.

4.3 Observed E-field enhancement as compared to LREF

In Fig. 6 and Fig. 7, we present the dust events that induced an enhanced electrical behaviour near the ground. The E-field strength measurements are averaged over 5 mins in order to be comparable with the lidar data. In the July 25th layer (Fig. 6), dust advection is recorded since the first morning hours and areas of increased particle concentration can be spotted from early noon. The δ_p profile signifies that the layer consists primarily of dust which descends after ~16:00 (UTC) and falls entirely below 2 km at ~18:30 (UTC), but the mean electric field (black line) remains above the reference field (red contoured line),

showing an increase when particle density is maximized towards noon and a small drop when dust concentration within the MABL becomes significant. A similar electrical behaviour was observed during the dust event of October 2018 that reached the PANGEA observatory. Large lofted particle concentrations are attributed to dust according to the mean δ_p values that reach up to ~25% - 27% (Fig. 7). For both cases, the mean E_z appears enhanced as compared to the LREF. According to the physical approximation of cylindrical charged areas (see Section 3.2), such an enhancement would be expected only when the lofted dust layer is electrically active and charge separation within the layer is prominent. From Fig. 5b, it becomes apparent that the external E-field is more sensitive to charge imbalances, even small ones, than to separation distance variations, hence a charge imbalance within these layers could drive the E-field above the fair weather values, as observed in the above cases, for even smaller charge separation distances.

4.4 Observed E-field reduction as compared to LREF

Several dust load cases were detected, both in Finokalia and Antikythera, where the near-ground electric field strength exhibits a decrease when compared to the local reference field and, particularly, when high dust particle concentrations were present. In the specific study, we select the cases of March 2018 and June 2019 in terms of the similar temporal injection of dust particles, large AOD values and similar layer progression throughout the day. From the δ_p profile (20% - 30%), we deduce that for both cases, the elevated layer between 2 and 4 km consists primarily of dust particles, while the decrease of δ_p towards the bottom of the layer is indicative of downward mixing inside the MABL, with marine particles of lower δ_ps. The mean E-field remains positive and well below the reference field, exhibiting an increase as dust injection initiates at ~09:00 (UTC) and then a decrease along the plume's progression (Fig. 8). Moreover, the bottom of the dust layer of the June 23rd case, seems to progressively move towards lower altitudes during late afternoon but the total dust load remains persistent. The effect of the dust plume on the electric field is clearly similar to the previous case in Finokalia, where the mean E-field remains positive and always below the LREF but appears to be increasing with rising dust concentrations. Following the 1D model outputs for such a case (see Section 3.1.1), this observed reduction could be attributed to either electrically neutral dust aloft or to electrically active dust with the charged regions in relatively small separation distances within the layer. Under the electrically active dust case, a charge imbalance of less than 10%, can be adequate to interpret the observed reduction of the E-field below the LREF for even smaller separation distances. But the detection of such an E-field reduction below the LREF cannot conclusively characterize the electrical activity of the dust layer aloft.

4.5 Reversed E-field polarity

If a reversed polarity E-field is observed (in our timeseries there were dust cases under which the field exhibited polarity reversal), with the opposite sign signifying that the field vector points upwards instead of downwards, then the investigated formalism is capable of explaining the reversal. As such, a similar cylindrical configuration could be assumed with the only difference being that the lower layer has to be negatively charged and the upper one, in the dipole case, to be positively charged.

Under this condition, the conclusions derived from the model remain the same. Therefore, such an indication of reversal is explained only via reversed separated cylindrical charges and again points that lofted dust has to be electrified.

5 Discussion

5.1 E-field dependence on the bottom charged area height

From the above results, the question that arises is whether the proximity of the lower cylinder, to the ground itself, is capable to reproduce the electric field enhancement feature above the LREF. It becomes clear that two mechanisms act upon the enhancement of the near-ground electric field. The first is the decrease of the contribution of the upper layer as it moves upwards due to the enhancement of the columnar resistance between the layer and the ground. The second is the increase of the contribution of the lower layer as it moves downwards, due to the decrease of the columnar resistance between the layer and the ground. The closer the lower layer is to the ground, the smaller the separation with the upper layer is required for the enhancement of the electric field.

In order to validate the influence of each parameter, we re-examine the ground E-field behaviour by keeping the lower cylinder at a fixed altitude of 2 km (close to the dust layer base, similarly to thundercloud activity e.g. Mallios and Pasko, 2012) and we, then, increase the separation distance. As observed in Fig. 10, the increasing separation distance causes the E-field to increase at the ground and when it becomes large enough (top and bottom right panels), the upper cylinder does no longer influence the ground E-field. At this point, for both balanced and imbalanced dipoles with cylinder radius larger than ∼40 km, the field converges to a constant value. This becomes clearer when comparing Fig. 10 with Fig. 4. When the separation distance is 400 m, the electric field at the ground is larger than the reference field in the case of Fig. 10, while at Fig. 4, separation distance equal to 400 m happens when the bottom layer is at 2.75 km. In this case, the field is lower than the reference value which indicates that the closer the bottom layer is to the ground, the smaller the separation distance needed for the enhancement of the ground electric field above the reference field. Moreover, the E-field value for zero separation distance is consistently below the calculated fair weather value. As such, observations of enhanced E-field above the fair weather values, for dust driven days, can be reproduced only when an electrically active dust layer is transported above the field mill.

If we assume that the bottom charged area is close to the lofted layer base, we would expect an increase to the ground electric field as the layer progressively moves towards lower altitudes. For the comparison of the E-field timeseries with the descending layer base (Fig. 11), we use the cross polarized component of the lidar signal at 532 nm, from which we can derive information on the vertical distribution of the aerosol layers. More specifically, we applied a methodology where the first derivative of the attenuated backscatter coefficient is used to determine layer boundaries (Flamant et al., 1997; Mattis et al., 2008). The local maximum and local minimum of the derivative are considered to be the bottom and top of the layer respectively. The agreement between the time-height displays of the attenuated backscatter coefficient and the corresponding gradient (Fig. 6 to Fig. 9 and Fig. 11) can be used to verify the results of the gradient method.

As seen in the July 2017, March 2018 and June 2019 dust events, there is an enhancement of the reconstructed mean E-field followed by the layer base progression towards the ground, for specific timeframes within the day. This could signify the presence of positive charges accumulated to the layer base.

5.2 Chauvenet criterion validity

In Section 2.2.2, we described the processing chain for the determination of the local fair weather days at both atmospheric remote sensing stations. The novelty of the approach lies to the fact that only signal processing constraints are used, without incorporating criteria of local meteorological parameters that could redefine the initial conditions for the total fair weather days determination (Harrison and Nicoll, 2018). Nonetheless, threshold values concerning these factors are subjective, and may vary from study to study, which leads to differences in the extracted fair weather days. The specific study proposes a mathematically strict approach with the imposition of the Chauvenet criterion, which exploits only the field mill data and has a physical impact on the dataset. Under fair weather days, the mean electric field is approximately constant and the fewer by far dust driven days as captured in both stations, which are about 10% of the days within a typical year for both stations, will not influence significantly the reconstructed mean field value, but will be well beyond the standard deviation. The Chauvenet criterion excludes the days with such high variations as outliers and, therefore, the methodology for the reconstruction of the local reference field is less biased to variations occurring in dust driven days.

5.3 Generalization of the cylindrical model and LREF methodology

The methodology followed for the calculation of the ground electric field can be expanded to the area away from the central axis of the charged cylinders. As the cylinder radius increases and the infinite plate regime is approached, effects due to charged layer edges that induce radial electric field components, do not impact the sensor axis for a larger horizontal extent of the charged layer. This expands the analytical calculation as it becomes valid within a band region further away from the cylinder center. In the small radius regime, the sensor becomes sensitive to edge effects and the edge field can be far stronger than the on-axis field. If we assume that a transient dust layer is transported with a mean wind speed of 10 m/s, implying a regional scale transport, then in a period of 2 hrs the edge will be 72 km away from the sensor axis (fast transits), a sufficient distance to not affect the vertical component of the electric field. Although these variations are present on the raw timeseries (observed peak activity in Fig. 6, Fig. 8 and Fig. 9), in the reconstruction of the LREF variations with timescales shorter than 6 hrs are the lower limit to the FFT input and are therefore excluded. This leaves the LREF unbiased to edge effects. Problems might be caused in our analysis in the case of very slowly moving dust layers, that are transported with wind speeds less than 1 m/s. Dust layer edge effects can provide basic information on the layer properties and could be incorporated in our cylindrical layer formalism, but this consists a subject of further investigation in the near future.

6 Summary and Conclusions

Near-ground electric field strength observations during Saharan dust advection over Greece exhibit three distinct responses of enhancement, reduction or sign reversal when compared to local fair weather values. In this paper, we present four cases of
500 transient dust events that influence the ground electric field recorded at two atmospheric remote sensing stations synergistically with a lidar system and a field mill electrometer. Moreover, this work attempts to use only ground-based atmospheric electricity instrumentation as a proxy for electrified dust detection, with characterization in terms of optical properties from lidar observations. To quantify the effect of charged dust particles, we implemented a reference electric field representing the local fair weather field, using long-term measured timeseries, and examine the possible physical mechanisms that could explain the
505 electric field behaviour. Our findings suggest that dust cases with the reconstructed mean E-field magnitude above the reference field indicate charge separation within the layer either as a balanced or imbalanced dipole (or a multipole) of charge layers, while when the mean field is completely below the reference field, dust electrical activity characterization is inconclusive. This ground electric field reduction below the local fair weather field can be attributed to either the conductivity reduction due to dust acting as a passive neutral element, where the greater the conductivity reduction the lesser the electric
510 field reduction, or to charge separation between areas of accumulated charge.

The electrified dust scheme is approximated either via the absence of dust charge separation or with thin cylindrical finite charge geometries (as opposed to infinite plate analogues) that allow explaining the electric field dependence on the layer height and the separation distance between the regions of charge accumulation. Both concepts have been suggested to explain the observed E-field responses at ground. However, there is no observational evidence up to now to validate the charge strata
515 morphology, which might be far from similar to the elevated layers morphology due to the charged dust particles complex transport dynamics. To constrain the modelling formalism proposed here, future research will include profiling of the columnar electrical properties of dust, deploying airborne platforms (balloons and UAVs) within the Saharan Air Layer during foreseen future experiments at Cyprus and Cape Verde within 2021.

Appendix A

520 **Dust layer acting as a passive element**

In Fig. A1, the dependence of the near ground electric field strength, $E_{z_0,layer}$ (red line), of an electrically neutral dust layer on the conductivity reduction factor, the scale height, the layer central height and the layer depth, as given in (11), is plotted and compared to the fair weather electric field E_{z_0} at ground (blue line) which is given by (7). E_{z_0} depends only on the scale height and decreases as l increases, while it remains constant for the other varying parameters as expected from equation (7).
525 The calculated fair weather field value of ~ 42 V/m, for the selected l, is comparable to the estimated value by Williams (2003) from Ohm's law, when dividing the globally integrated conduction current density by the mean atmospheric electrical conductivity at ground ($J_{z_0} \approx 2x10^{-12} A/m^2, \sigma_0 \approx 5x10^{-14} S/m$) and assuming an exponentially increasing conductivity

profile above the Earth's surface (Haldoupis et al., 2017). We note that this globally averaged value of E_{z_0} is much less from the typically measured which is around 100 V/m (e.g. Corney et al., 2003; Reddell et al., 2004). We believe that the average value is more suitable for global calculations, because it incorporates the variations of the conductivity distribution around the Earth. On the other hand, the typical value is tied to the location of the measurement, and it varies at different locations as the conductivity distribution changes. Consequently, $E_{z_0,layer}$ exhibits the greatest variation with the reduction factor n, meaning that atmospheric conductivity reduction is the predominant factor that affects the E-field strength by largely lowering it.

Authors Contribution: VD supervised the installation of the FM in both stations, collected and processed the data, constructed the reference field, provided physical input to the model and to the measurements' interpretation, plotted the lidar data and prepared the paper with contributions from all co-authors. SM conceptualized the model formalism and the processing chain of the reference field, also provided the key physical interpretation of the measurements. VA directed the preparation of the paper, supervised the study, offered his specialty in lidar data interpretation and gave insight to the E-field measurements. JU kindly conferred the FM, co-supervised the study and provided scientific consultation on both model outputs and E-field measurements. GH installed the FM on both stations, ensured the continuous data retrieval and gave insight to the E-field measurements. AG operated the lidar and supervised the data retrieval, provided the processed lidar data, along with dust layer base plots and aided on their interpretation. IT provided the VLDR data and helped on the selection of the dust cases according to these. Lastly, KT provided valuable scientific consultation concerning the E-field data, model assumptions and correlation to the dust layer proximity to the ground.

Acknowledgments: This research was supported by data and services obtained from the PANhellenic GEophysical Observatory of Antikythera (PANGEA) of NOA. The authors would like to acknowledge support of this work by the project "PANhellenic infrastructure for Atmospheric Composition and climatE change" (MIS 5021516) which is implemented under the Action "Reinforcement of the Research and Innovation Infrastructure", funded by the Operational Programme "Competitiveness, Entrepreneurship and Innovation" (NSRF 2014-2020) and co-financed by Greece and the European Union (European Regional Development Fund). We are grateful to EARLINET (https://www.earlinet.org/) and ACTRIS (https://www.actris.eu) for the data collection, calibration, processing and dissemination. VD would like to thank Dr. Eleni Marinou for distributing the processing algorithm for the attenuated backscatter lidar retrievals. VD would also like to thank Prof. Charmandaris for his insightful comments and Dr. Nikos Kalivitis for his help in the data retrieval from Finokalia.

Financial Support: This research was supported by D-TECT (Grant Agreement No. 725698) funded by the European Research Council (ERC) under the European Union's Horizon 2020 research and innovation programme. VD would like to acknowledge that this research is also co-financed by Greece and the European Union (European Social Fund- ESF) through the Operational Programme «Human Resources Development, Education and Lifelong Learning» in the context of the project "Strengthening Human Resources Research Potential via Doctorate Research" (MIS-5000432), implemented by the State

Scholarships Foundation (IKY)» and supported by the A. G. Leventis Foundation scholarship. Support was provided also from the Stavros Niarchos Foundation (SNF) in the form of a student scholarship. KT acknowledges funding from the European Research Council (ERC) under the European Unions Horizon 2020 research and innovation programme under Grant Agreement No. 771282.

565

Conflicts of Interest: The authors declare no conflict of interest.

References

570   Anisimov, S. V., Afinogenov, K. V. and Shikhova, N. M.: Dynamics of undisturbedmidlatitude atmospheric electricity: From observations to scaling, Radiophys. Quantum Electron., 56(11–12), 709–722, doi:10.1007/s11141-014-9475-z, 2014.

Anisimov, S. V., Galichenko, S. V. and Mareev, E. A.: Electrodynamic properties and height of atmospheric convective boundary layer, Atmos. Res., 194, 119–129, doi:10.1016/j.atmosres.2017.04.012, 2017.

Bailey, J., Ulanowski, Z., Lucas, P. W., Hough, J. H., Hirst, E. and Tamura, M.: The effect of airborne dust on astronomical

575   polarization measurements, Mon. Not. R. Astron. Soc., 386(2), 1016–1022, doi:10.1111/j.1365-2966.2008.13088.x, 2008.

Baumgaertner, A. J. G., Lucas, G. M., Thayer, J. P. and Mallios, S. A.: On the role of clouds in the fair weather part of the global electric circuit, Atmos. Chem. Phys., 14(16), 8599–8610, doi:10.5194/acp-14-8599-2014, 2014.

Bering, E. A., Few, A. A. and Benbrook, J. R.: The global electric circuit, Phys. Today, 51(10), 24–30, doi:10.1063/1.882422, 1998.

580   Chubb, J.: The measurement of atmospheric electric fields using pole mounted electrostatic fieldmeters, J. Electrostat., 72(4), 295–300, doi:10.1016/j.elstat.2014.05.002, 2014.

Chubb, J.: Comparison of atmospheric electric field measurements by a pole mounted fieldmeter and by a horizontal wire antenna, J. Electrostat., 73, 1–5, doi:10.1016/j.elstat.2014.10.003, 2015.

Corney, R. C., Burns, G. B., Michael, K., Frank-Kamenetsky, A. V., Troshichev, O. A., Bering, E. A., Papitashvili, V. O.,

585   Breed, A. M. and Duldig, M. L.: The influence of polar-cap convection on the geoelectric field at Vostok, Antarctica, J. Atmos. Solar-Terrestrial Phys., 65(3), 345–354, doi:10.1016/S1364-6826(02)00225-0, 2003.

van der Does, M., Knippertz, P., Zschenderlein, P., Giles Harrison, R. and Stuut, J. B. W.: The mysterious long-range transport of giant mineral dust particles, Sci. Adv., 4(12), 1–9, doi:10.1126/sciadv.aau2768, 2018.

Duff, N. and Lacks, D. J.: Particle dynamics simulations of triboelectric charging in granular insulator systems, J. Electrostat.,

590   66(1–2), 51–57, doi:10.1016/j.elstat.2007.08.005, 2008.

Engelmann, R., Kanitz, T., Baars, H., Heese, B., Althausen, D., Skupin, A., Wandinger, U., Komppula, M., Stachlewska, I. S., Amiridis, V., Marinou, E., Mattis, I., Linné, H. and Ansmann, A.: The automated multiwavelength Raman polarization and water-vapor lidar PollyXT: The neXT generation, Atmos. Meas. Tech., 9(4), 1767–1784, doi:10.5194/amt-9-1767-2016, 2016.

Esposito, F., Molinaro, R., Popa, C. I., Molfese, C., Cozzolino, F., Marty, L., Taj-Eddine, K., Di Achille, G., Franzese, G.,

595   Silvestro, S. and Ori, G. G.: The role of the atmospheric electric field in the dust-lifting process, Geophys. Res. Lett., 43(10), 5501–5508, doi:10.1002/2016GL068463, 2016.

Ette, A. I. I.: The effect of the Harmattan dust on atmospheric electric parameters, J. Atmos. Terr. Phys., 33(2), 295–300, doi:10.1016/0021-9169(71)90208-X, 1971.

Flamant, C., Pelon, J., Flamant, P. H. and Durand, P.: Lidar determination of the entrainment zone thickness at the top of the

600   unstable marine atmospheric boundary layer, Boundary-Layer Meteorol., 83(2), 247–284, doi:10.1023/A:1000258318944, 1997.

Forward, K. M., Lacks, D. J. and Mohan Sankaran, R.: Particle-size dependent bipolar charging of Martian regolith simulant,

Geophys. Res. Lett., 36(13), 1–5, doi:10.1029/2009GL038589, 2009.

Freier G. D.: The Electric Field of a Large Dust Devil, October, (10), 1960–1960, 1960.

605 Freudenthaler, V., Esselborn, M., Wiegner, M., Heese, B., Tesche, M., Ansmann, A., Müller, D., Althausen, D., Wirth, M., Fix, A., Ehret, G., Knippertz, P., Toledano, C., Gasteiger, J., Garhammer, M. and Seefeldner, M.: Depolarization ratio profiling at several wavelengths in pure Saharan dust during SAMUM 2006, Tellus, Ser. B Chem. Phys. Meteorol., 61(1), 165–179, doi:10.1111/j.1600-0889.2008.00396.x, 2009.

Griffiths, D. J.: Instructor's Solution Manual for Introduction to Electrodynamics, 4th Edition, Reed College, Pearson, 2013.

610 Gringel W. and Mulheisen R.: Sahara dust concentration in the troposphere over the north Atlantic derived from measurements of air conductivity Beitr. Phys. Atmos. 51 121–8, 1978.

Gringel, W., J. M. Rosen, and D. J. Hoffmann.: Electrical structure from 0 to 30 km, in The Earth Electrical Environment, edited by E. P. Krider and R. G. Robie, pp. 166-182, Nat. Acad. Press, Washington, D.C., 1986.

Gunn, R.: Diffusion Charging of Atmospheric Droplets By Ions, and the Resulting Combination Coefficients, J. Meteorol.,
615 11(5), 339–347, doi:10.1175/1520-0469(1954)011<0339:dcoadb>2.0.co;2, 1954.

Haarig, M., Ansmann, A., Althausen, D., Klepel, A., Groß, S., Freudenthaler, V., Toledano, C., Mamouri, R. E., Farrell, D. A., Prescod, D. A., Marinou, E., Burton, S. P., Gasteiger, J., Engelmann, R. and Baars, H.: Triple-wavelength depolarization-ratio profiling of Saharan dust over Barbados during SALTRACE in 2013 and 2014, Atmos. Chem. Phys., 17(17), 10767–10794, doi:10.5194/acp-17-10767-2017, 2017.

620 Haldoupis, C., Rycroft, M., Williams, E. and Price, C.: Is the "Earth-ionosphere capacitor" a valid component in the atmospheric global electric circuit?, J. Atmos. Solar-Terrestrial Phys., 164(August), 127–131, doi:10.1016/j.jastp.2017.08.012, 2017.

Harrison, R. G.: Ion-aerosol-cloud processes in the lower atmosphere, Rev. Geophys., 41(3), 1012, doi:10.1029/2002RG000114, 2003.

625 Harrison, R. G.: The Carnegie Curve, , (July 2012), 209–232, doi:10.1007/s10712-012-9210-2, 2013.

Harrison, R. G. and Ingram, W. J.: Air-earth current measurements at Kew, London, 1909-1979, Atmos. Res., 76(1–4), 49–64, doi:10.1016/j.atmosres.2004.11.022, 2005.

Harrison, R. G. and Nicoll, K. A.: Fair weather criteria for atmospheric electricity measurements, J. Atmos. Solar-Terrestrial Phys., 179(February), 239–250, doi:10.1016/j.jastp.2018.07.008, 2018.

630 Harrison, R. G., Nicoll, K. A., Ulanowski, Z. and Mather, T. A.: Self-charging of the Eyjafjallajökull volcanic ash plume, Environ. Res. Lett., 5(2), 3–7, doi:10.1088/1748-9326/5/2/024004, 2010.

Harrison, R. G., Barth, E., Esposito, F., Merrison, J., Montmessin, F., Aplin, K. L., Borlina, C., Berthelier, J. J., Déprez, G., Farrell, W. M., Houghton, I. M. P., Renno, N. O., Nicoll, K. A., Tripathi, S. N. and Zimmerman, M.: Applications of Electrified Dust and Dust Devil Electrodynamics to Martian Atmospheric Electricity, Space Sci. Rev., 203(1–4), 299–345,
635 doi:10.1007/s11214-016-0241-8, 2016.

Harrison, R. G., Nicoll, K. A., Marlton, G. J., Ryder, C. L. and Bennett, A. J.: Saharan dust plume charging observed over the

UK, Environ. Res. Lett., 13(5), doi:10.1088/1748-9326/aabcd9, 2018.

Ilin, N. V., Slyunyaev, N. N. and Mareev, E. A.: Toward a Realistic Representation of Global Electric Circuit Generators in Models of Atmospheric Dynamics, J. Geophys. Res. Atmos., 125(6), 1–24, doi:10.1029/2019JD032130, 2020.

640 Inculet, I. I., Castle, G. S. P. and Aartsen, G.: Generation of bipolar electric fields during industrial handling of powders, Chem. Eng. Sci., 61(7), 2249–2253, doi:10.1016/j.ces.2005.05.005, 2006.

Kalinin, A. V., Slyunyaev, N. N., Mareev, E. A. and Zhidkov, A. A.: Stationary and nonstationary models of the global electric circuit: Well-posedness, analytical relations, and numerical implementation, Izv. - Atmos. Ocean Phys., 50(3), 314–322, doi:10.1134/S0001433814030074, 2014.

645 Kamra,   a. K.: Measurements of the electrical properties of dust storms, J. Geophys. Res., 77(30), 5856, doi:10.1029/JC077i030p05856, 1972.

Kanagy, S. P. and Mann, C. J.: Electrical properties of eolian sand and silt, Earth Sci. Rev., 36(3–4), 181–204, doi:10.1016/0012-8252(94)90057-4, 1994.

Katz, S., Yair, Y., Price, C., Yaniv, R., Silber, I., Lynn, B. and Ziv, B.: Electrical properties of the 8–12th September, 2015
650 massive dust outbreak over the Levant, Atmos. Res., 201(November 2017), 218–225, doi:10.1016/j.atmosres.2017.11.004, 2018.

Kok, J. F. and Renno, N. O.: Enhancement of the emission of mineral dust aerosols by electric forces, Geophys. Res. Lett., 33(19), 2–6, doi:10.1029/2006gl026284, 2006.

Kourtidis, K., Szabóné André, K., Karagioras, A., Nita, I. A., Sátori, G., Bór, J. and Kastelis, N.: The influence of circulation
655 weather types on the exposure of the biosphere to atmospheric electric fields, Int. J. Biometeorol., doi:10.1007/s00484-020-01923-y, 2020.

Krehbiel, P. R., Riousset, J. A., Pasko, V. P., Thomas, R. J., Rison, W., Stanley, M. A. and Edens, H. E.: Upward electrical discharges from thunderstorms, Nat. Geosci., 1(4), 233–237, doi:10.1038/ngeo162, 2008.

Lacks, D. J. and Shinbrot, T.: Long-standing and unresolved issues in triboelectric charging, Nat. Rev. Chem., 3(8), 465–476,
660 doi:10.1038/s41570-019-0115-1, 2019.

Lelieveld, J., Berresheim, H., Borrmann, S., Crutzen, P. J., Dentener, F. J., Fischer, H., Feichter, J., Flatau, P. J., Heland, J., Holzinger, R., Korrmann, R., Lawrence, M. G., Levin, Z., Markowicz, K. M., Mihalopoulos, N., Minikin, A., Ramanathan, V., De Reus, M., Roelofs, G. J., Scheeren, H. A., Sciare, J., Schlager, H., Schultz, M., Siegmund, P., Steil, B., Stephanou, E. G., Stier, P., Traub, M., Warneke, C., Williams, J. and Ziereis, H.: Global air pollution crossroads over the Mediterranean,
665 Science (80-.)., 298(5594), 794–799, doi:10.1126/science.1075457, 2002.

Long, Z. and Yao, Q.: Evaluation of various particle charging models for simulating particle dynamics in electrostatic precipitators, J. Aerosol Sci., 41(7), 702–718, doi:10.1016/j.jaerosci.2010.04.005, 2010.

Mallios, S. A. and Pasko, V. P.: Charge transfer to the ionosphere and to the ground during thunderstorms, J. Geophys. Res. Sp. Phys., 117(8), 1–16, doi:10.1029/2011JA017061, 2012.

670 Mallios, S. A., Daskalopoulou, V. and Amiridis, V.: Orientation of non spherical prolate dust particles moving vertically in

the Earth's atmosphere, J. Aerosol Sci., 151(August 2020), 105657, doi:10.1016/j.jaerosci.2020.105657, 2021.

Mattis, I., Müller, D., Ansmann, A., Wandinger, U., Preißler, J., Seifert, P. and Tesche, M.: Ten years of multiwavelength Raman lidar observations of free-tropospheric aerosol layers over central Europe: Geometrical properties and annual cycle, J. Geophys. Res. Atmos., 113(20), 1–19, doi:10.1029/2007JD009636, 2008.

675   Nicoll, K., Harrison, G., Marlton, G. and Airey, M.: Consistent dust electrification from Arabian Gulf sea breezes, Environ. Res. Lett., 15(8), doi:10.1088/1748-9326/ab9e20, 2020.

Nicoll, K. A., Harrison, R. G. and Ulanowski, Z.: Observations of Saharan dust layer electrification, Environ. Res. Lett., 6(1), 1–8, doi:10.1088/1748-9326/6/1/014001, 2011.

Reddell, B. D., Benbrook, J. R., Bering, E. A., Cleary, E. N. and Few, A. A.: Seasonal variations of atmospheric electricity

680   measured at Amundsen-Scott South Pole Station, J. Geophys. Res. Sp. Phys., 109(A9), 1–17, doi:10.1029/2004JA010536, 2004.

Renno, N. O. and Kok, J. F.: Electrical activity and dust lifting on earth, Mars, and beyond, Space Sci. Rev., 137(1–4), 419–434, doi:10.1007/s11214-008-9377-5, 2008.

Riousset, J. A., Pasko, V. P., Krehbiel, P. R., Thomas, R. J. and Rison, W.: Three-dimensional fractal modeling of intracloud

685   lightning discharge in a New Mexico thunderstorm and comparison with lightning mapping observations, J. Geophys. Res. Atmos., 112(15), 1–17, doi:10.1029/2006JD007621, 2007.

Rycroft, M. J., Harrison, R. G., Nicoll, K. A. and Mareev, E. A.: An overview of earth's global electric circuit and atmospheric conductivity, Space Sci. Rev., 137(1–4), 83–105, doi:10.1007/s11214-008-9368-6, 2008.

Ryder, C. L., Marenco, F., Brooke, J. K., Estelles, V., Cotton, R., Formenti, P., McQuaid, J. B., Price, H. C., Liu, D., Ausset,

690   P., Rosenberg, P., Taylor, J. W., Choularton, T., Bower, K., Coe, H., Gallagher, M., Crosier, J., Lloyd, G., Highwood, E. J. and Murray, B. J.: Coarse mode mineral dust size distributions, composition and optical properties from AER-D aircraft measurements over the Tropical Eastern Atlantic, Atmos. Chem. Phys. Discuss., 98, 1–49, doi:10.5194/acp-2018-739, 2018.

Siingh, D., Gopalakrishnan, V., Singh, R. P., Kamra, A. K., Singh, S., Pant, V., Singh, R. and Singh, A. K.: The atmospheric global electric circuit: An overview, Atmos. Res., 84(2), 91–110, doi:10.1016/j.atmosres.2006.05.005, 2007.

695   Silva, H. G., Lopes, F. M., Pereira, S., Nicoll, K., Barbosa, S. M., Conceição, R., Neves, S., Harrison, R. G. and Collares Pereira, M.: Saharan dust electrification perceived by a triangle of atmospheric electricity stations in Southern Portugal, J. Electrostat., 84, 106–120, doi:10.1016/j.elstat.2016.10.002, 2016.

Solomos, S., Kalivitis, N., Mihalopoulos, N., Amiridis, V., Kouvarakis, G., Gkikas, A., Binietoglou, I., Tsekeri, A., Kazadzis, S., Kottas, M., Pradhan, Y., Proestakis, E., Nastos, P. T. and Marenco, F.: From tropospheric folding to Khamsin and Foehn

700   winds: How atmospheric dynamics advanced a record-breaking dust episode in Crete, Atmosphere (Basel)., 9(7), doi:10.3390/atmos9070240, 2018.

Stolzenburg, M. and Marshall, T. C.: Charge structure and dynamics in thunderstorms, Space Sci. Rev., 137(1–4), 355–372, doi:10.1007/s11214-008-9338-z, 2008.

Tegen, I., Hollrig, P., Chin, M., Fung, I., Jacob, D. and Penner, J.: Contribution of different aerosol species to the global aerosol

705   extinction optical thickness: Estimates from model results, J. Geophys. Res. Atmos., 102(20), 23895–23915, doi:10.1029/97jd01864, 1997.

Tinsley, B. A. and Zhou, L.: Initial results of a global circuit model with variable stratospheric and tropospheric aerosols, , 111(August), 1–23, doi:10.1029/2005JD006988, 2006.

Ulanowski, Z., Bailey, J., Lucas, P., Hough, J. and Hirst, E.: Alighnment of atmospheric mineral dust due to electric field,
710   Atmos. Chem. Phys., 7, 6161–6173, 2007.

Veselovskii, I., Goloub, P., Podvin, T., Bovchaliuk, V., Derimian, Y., Augustin, P., Fourmentin, M., Tanre, D., Korenskiy, M., Whiteman, D. N., Diallo, A., Ndiaye, T., Kolgotin, A. and Dubovik, O.: Retrieval of optical and physical properties of African dust from multiwavelength Raman lidar measurements during the SHADOW campaign in Senegal, Atmos. Chem. Phys., 16(11), 7013–7028, doi:10.5194/acp-16-7013-2016, 2016.

715   Veselovskii, I., Hu, Q., Goloub, P., Podvin, T., Korenskiy, M., Derimian, Y., Legrand, M. and Castellanos, P.: Variability in lidar-derived particle properties over West Africa due to changes in absorption: Towards an understanding, Atmos. Chem. Phys., 20(11), 6563–6581, doi:10.5194/acp-20-6563-2020, 2020.

Waitukaitis, S. R., Lee, V., Pierson, J. M., Forman, S. L. and Jaeger, H. M.: Size-dependent same-material tribocharging in insulating grains, Phys. Rev. Lett., 112(21), 1–5, doi:10.1103/PhysRevLett.112.218001, 2014.

720   Whitby K. T., Liu B. Y. H.: The electrical behaviour of aerosols, Aerosol Science, C. N. Davies, Ed., Academic Press, 1966.

Williams, E. R.: The global electrical circuit: A review, Atmos. Res., 91(2–4), 140–152, doi:10.1016/j.atmosres.2008.05.018, 2009.

Wright, H. L.: The influence of atmospheric suspensoids upon the earth's electric field as indicated by observations at kew observatory, Proc. Phys. Soc., 45(2), 152–171, doi:10.1088/0959-5309/45/2/303, 1933.

725   Yair, Y., Katz, S., Yaniv, R., Ziv, B. and Price, C.: An electrified dust storm over the Negev desert, Israel, Atmos. Res., 181, 63–71, doi:10.1016/j.atmosres.2016.06.011, 2016.

Yaniv, R., Yair, Y., Price, C. and Katz, S.: Local and global impacts on the fair-weather electric field in Israel, Atmos. Res., 172–173, 119–125, doi:10.1016/j.atmosres.2015.12.025, 2016.

Yaniv, R., Yair, Y., Price, C., Mkrtchyan, H., Lynn, B. and Reymers, A.: Ground-based measurements of the vertical E-field
730   in mountainous regions and the "Austausch" effect, Atmos. Res., 189, 127–133, doi:10.1016/j.atmosres.2017.01.018, 2017.

Zhang, H. and Zhou, Y. H.: Reconstructing the electrical structure of dust storms from locally observed electric field data, Nat. Commun., 11(1), doi:10.1038/s41467-020-18759-0, 2020.

Zheng, X.-J.: Electrification of wind-blown sand: Recent advances and key issues, Eur. Phys. J. E, 36(12), 138, doi:10.1140/epje/i2013-13138-4, 2013.

735   Zhou, L. and Tinsley, B. A.: Production of space charge at the boundaries of layer clouds, J. Geophys. Res. Atmos., 112(11), 1–17, doi:10.1029/2006JD007998, 2007.
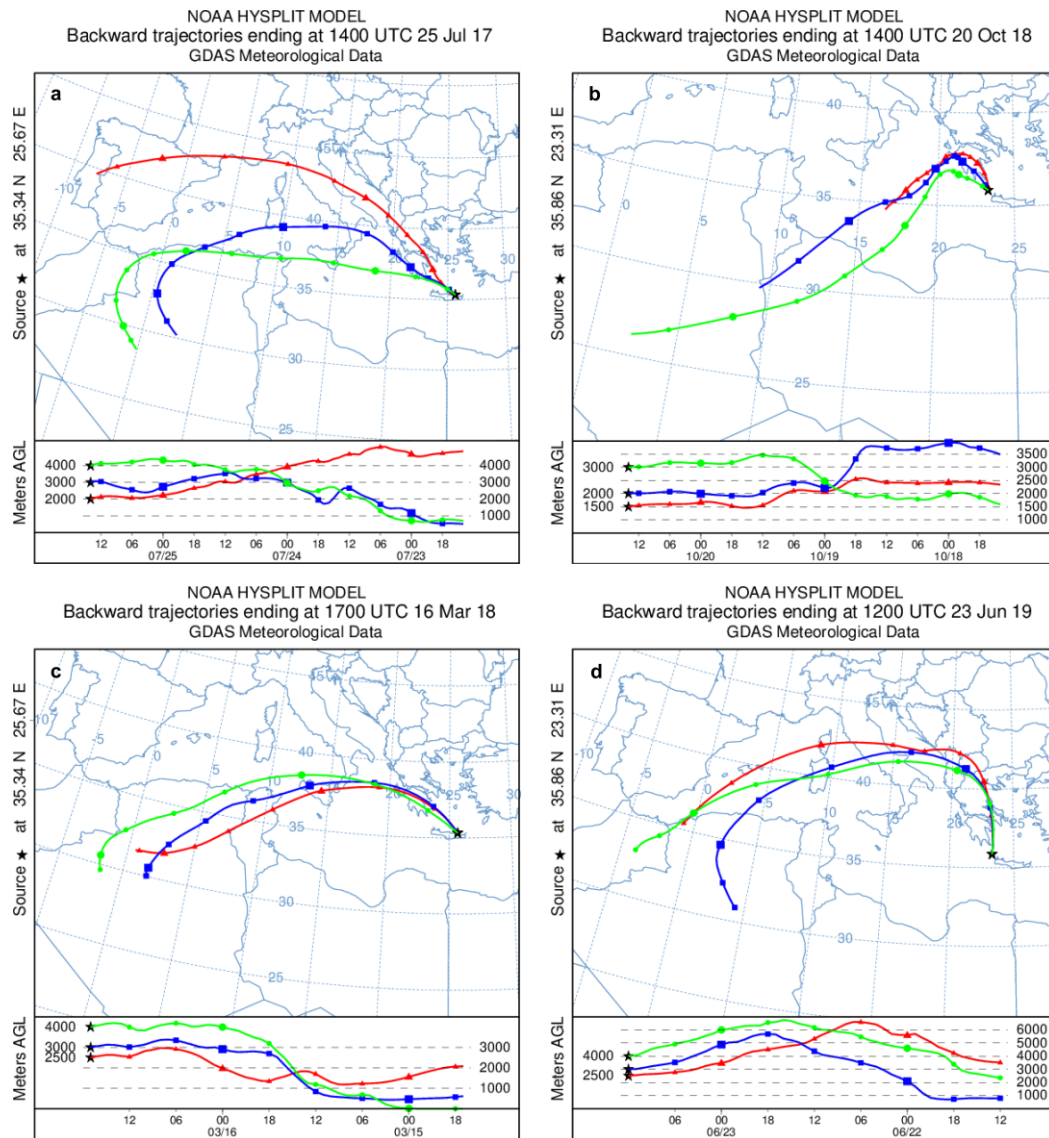
Fig. 1. NOAA HYSPLIT back trajectories for: **(a)** 25/07/2017 – 72 hrs (Fin.), **(b)** 20/10/2018 – 72 hrs (Antik.), **(c)** 16/03/2018 – 48 hrs (Fin.) and **(d)** 23/06/2019 – 48 hrs (Antik.) backward propagation of air masses.
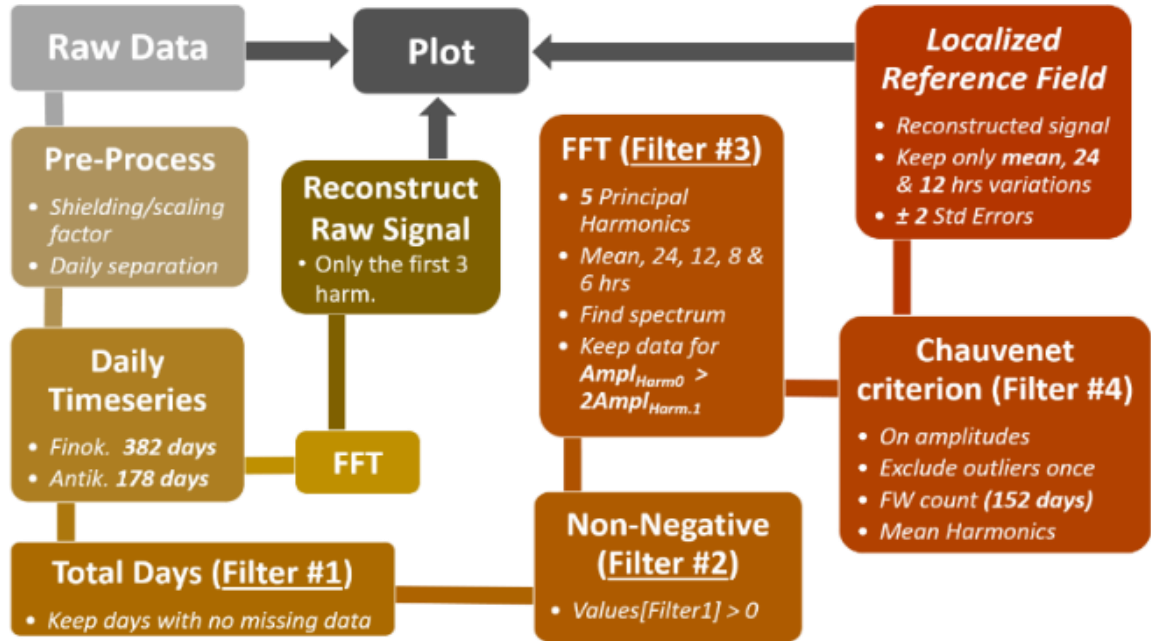
Fig. 2. Signal processing chain for: (i) the derivation of the Localized Reference Electric Field (LREF) that represents the local fair weather conditions and (ii) the derivation of the daily mean electric field under dust driven days. The LREF is compared to the mean electric field values in order to assess the electric field behavior.
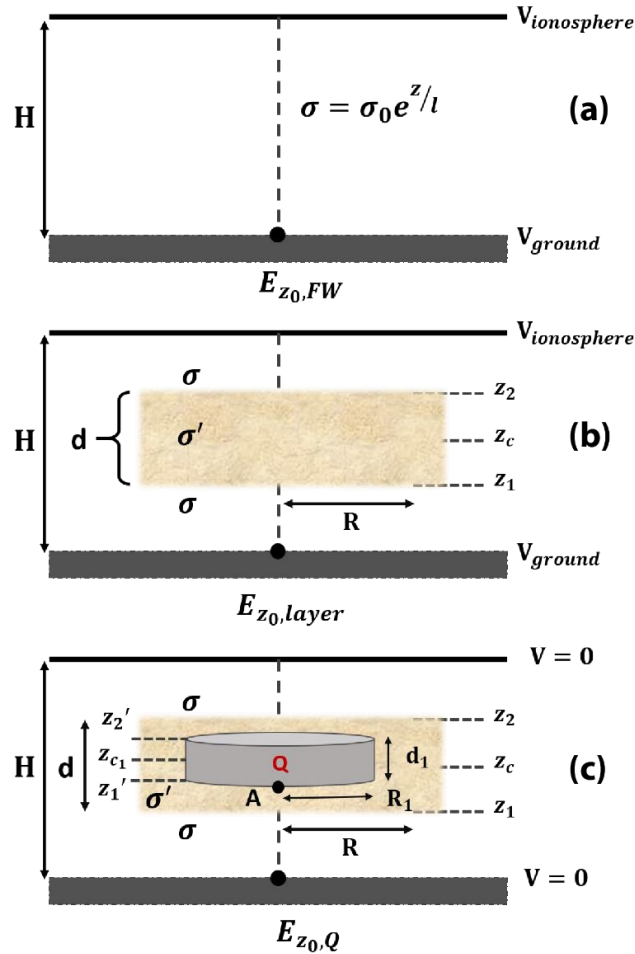
Fig. 3. Schematic of the formalism for the calculation of the steady state surface electric field under: (a) fair weather conditions, (b) the presence of an electrically neutral dust layer which reduces conductivity σ' and (c) the hypothesis of a cylindrical charged monopole within the dust layer. The monopole case is a superposition of the electrically neutral dust layer with the charged cylinder within a bounded atmospheric potential.

Table 1. Dust layer central height and depth, as derived from the PLDR profiles.

Dust Outbreak	z_{c_i} (km)	d_i (km)
25/07/2017 (Fin.)	3	4
20/10/2018 (Ant.)	3	4
16/03/2018 (Fin.)	3.5	2.5
23/06/2019 (Ant.)	3.5	3
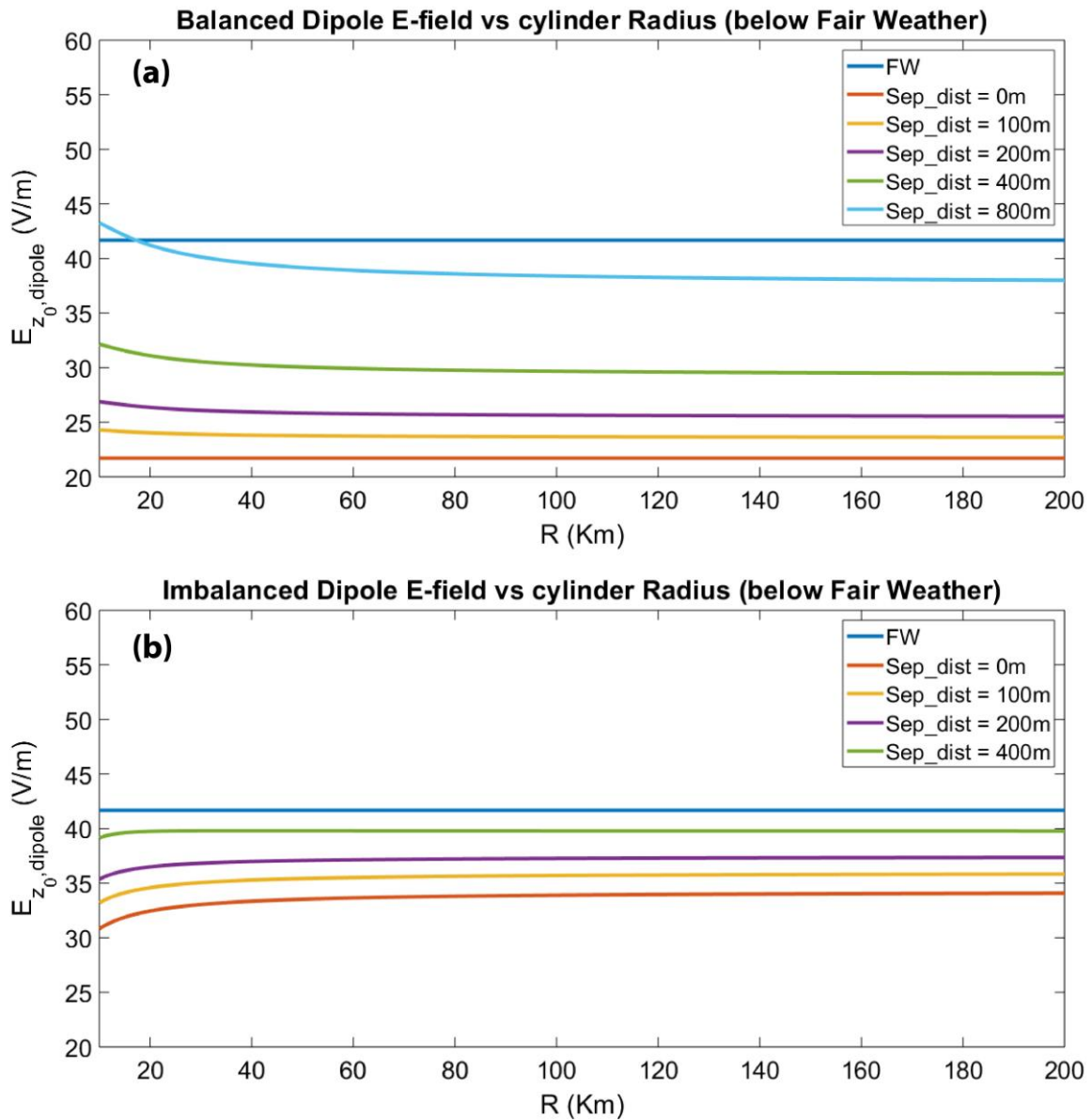
765

Fig. 4. Vertical electric field strength at ground level, $E_{z_0,dipole}$, below the fair weather field, for a dipole of: (a) finite uniformly charged cylinders and (b) non uniformly charged cylinders exhibiting charge imbalance, within an elevated dust layer as a function of the cylinder radius R. $E_{z_0,dipole}$ is calculated for separation distances of 0 (electrically neutral dust), 100, 200, 400 and 800 m (balanced dipole case only) between the charged layers. As the separation distance increases, the E-field increases due to the stronger

770 influence of the lower cylinder to the surface resistance as it moves towards the ground. In (b), the dipole exhibits charge imbalance as a relative charge density difference of 8%, with the upper negative cylinder having smaller charge density. As the charged layers move apart the E-field increases more rapidly than in (a) for the same separation distances, since the influence of the upper cylinder is dominant. The enhancement effect in both cases is not significant enough to overcome the fair weather values.
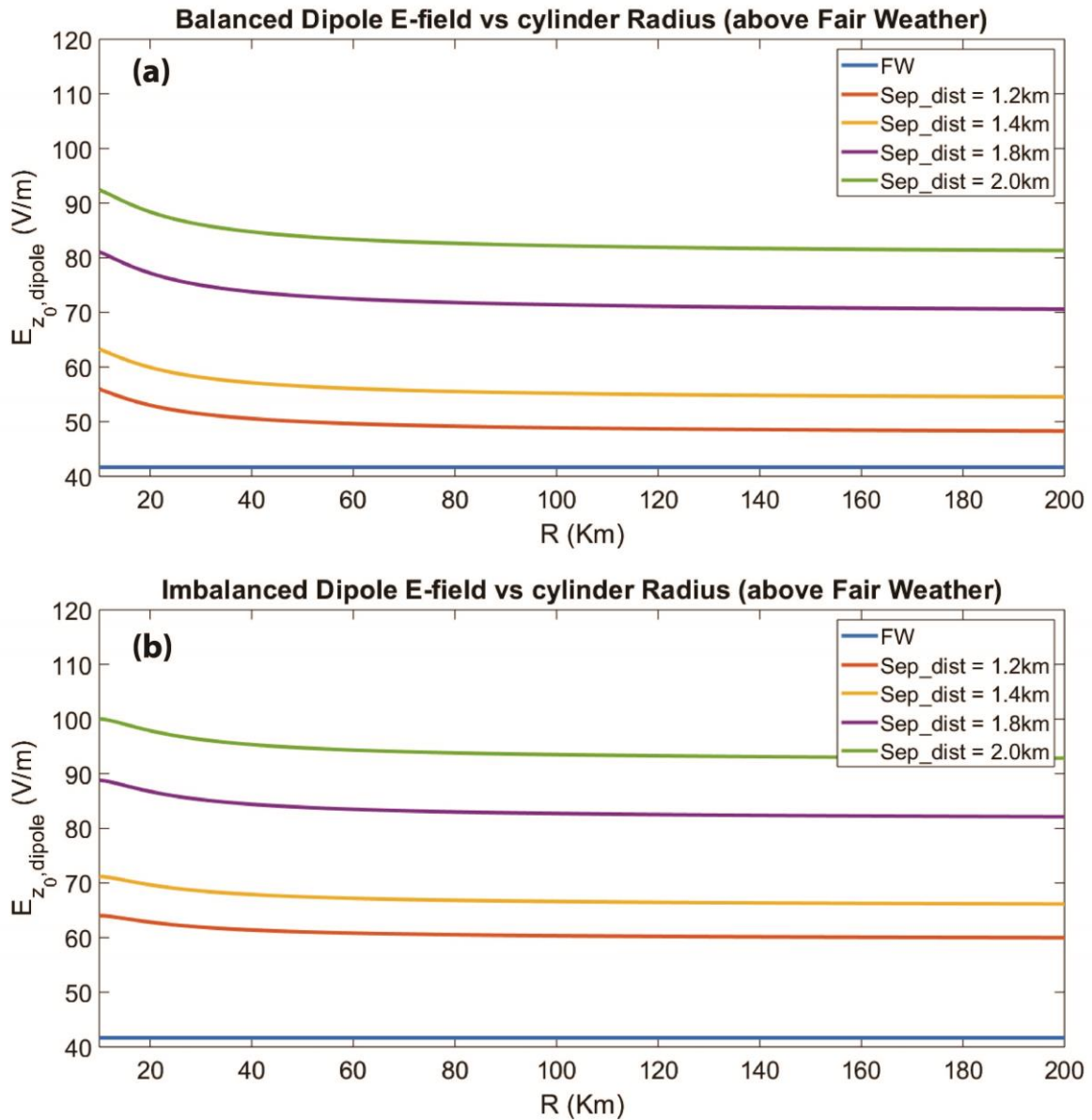
Fig. 5. Vertical electric field strength at ground level, $E_{z_0,dipole}$, for a dipole of: (a) finite uniformly charged cylinders and (b) non uniformly charged cylinders exhibiting charge imbalance, within an elevated dust layer as a function of the cylinder radius *R*. $E_{z_0,dipole}$ is calculated for separation distances over 1 km between the two charged layers. The influence of the lower cylinder to the ground E-field becomes more prominent as the separation distance increases. In (b), the dipole exhibits charge imbalance as a relative charge density difference of 8%, with the upper negative cylinder having smaller charge density. As the charged layers move apart the E-field increases more rapidly than in (a) for the same separation distances, since the influence of the upper cylinder is dominant. For these separation distances, the enhancement effect in both cases is significant enough to overcome the fair weather values.

Electric Field strength vs Attenuated Backscatter Coefficient at 532nm - July 25ᵗʰ 2017, Finokalia
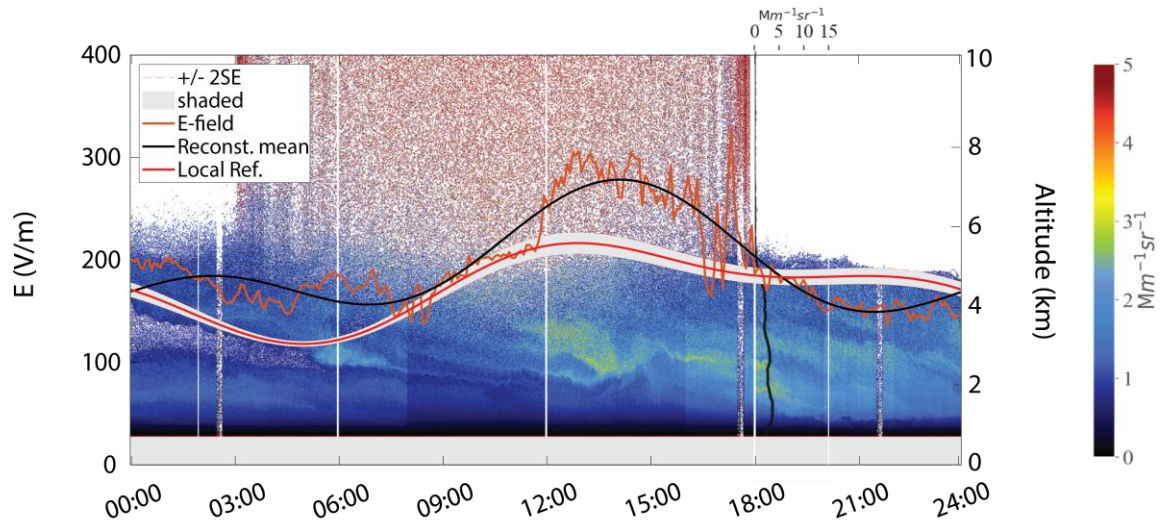
Polly^XT Volume Linear Depolarization Ratio at 532nm - July 25ᵗʰ 2017, Finokalia

Time of Day (UTC)
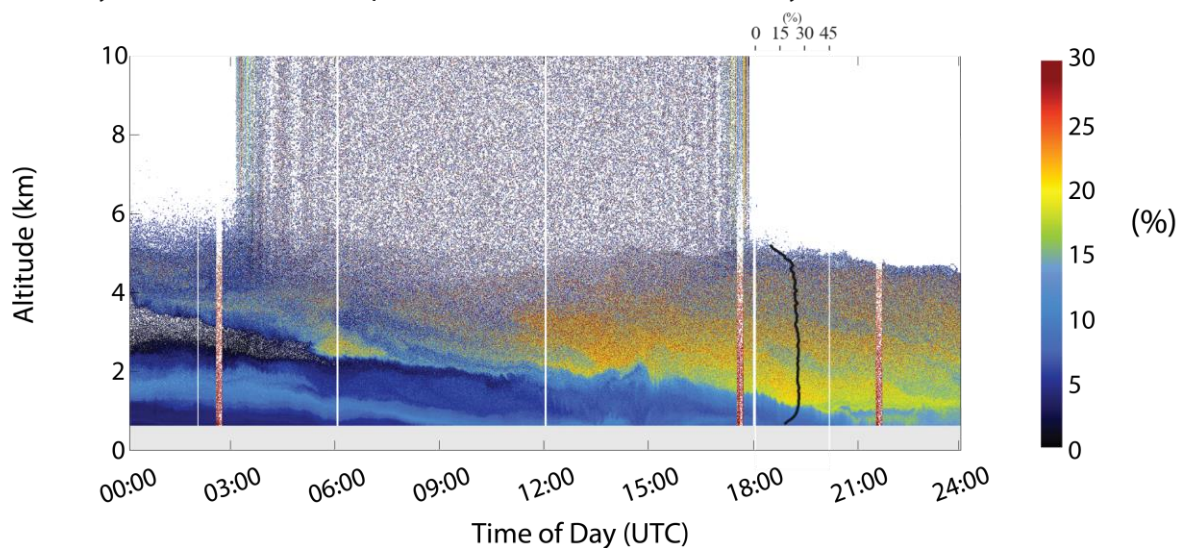
Fig. 6. **Top panel****: Timeseries of the vertical electric field strength (orange), the Localized Reference Electric Field (red) and the reconstructed mean electric field variation (black) plotted with the time-height evolution of the attenuated backscatter coefficient (Mm⁻¹sr⁻¹) and the particle backscatter coefficient (β) profile (Mm⁻¹sr⁻¹, black vertical line) averaged between 18:00 and 21:00 (UTC), for the 25/07/2017 dust layer in Finokalia station. Areas of increased particle concentration are denoted with reddish tones, while the β values are between 3 to 4 (Mm⁻¹sr⁻¹). The mean E-field appears enhanced and is above the reference field. **Bottom panel**: Volume Linear Depolarization Ratio (δ_v, %) for the same dust layer as obtained from the Polly^XT lidar and the Particle Linear Depolarization Ratio (δ_p, %) profile (black vertical line). High δ_v values (>17%) are indicative of dust particle presence and δ_p values between 25% - 30% in the afternoon are characteristic of pure dust.**

Electric Field strength vs Attenuated Backscatter Coefficient at 532nm - October 20th 2018, Antikythera
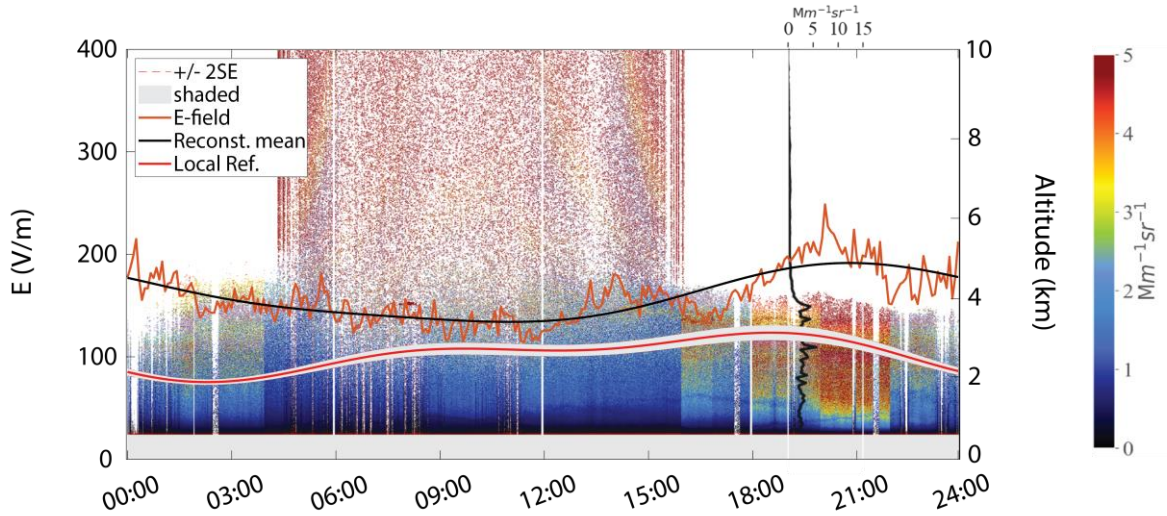
Polly^{XT} Volume Linear Depolarization Ratio at 532nm - October 20th 2018, Antikythera
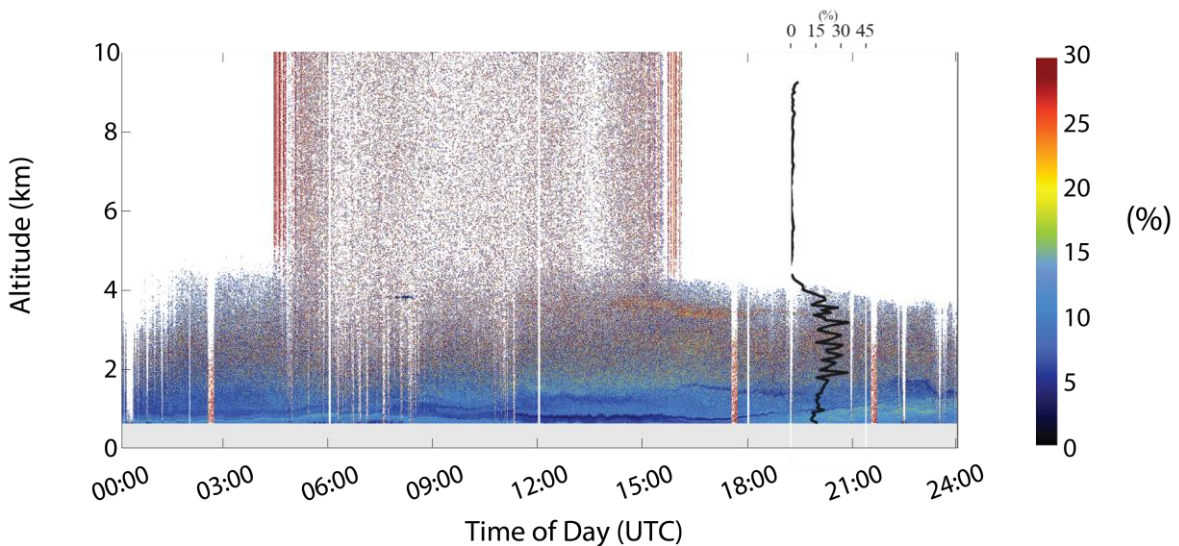
Fig. 7. Top panel: Timeseries of the vertical electric field strength (orange), the Localized Reference Electric Field (red) and the reconstructed mean electric field variation (black) plotted with the time-height plots of the attenuated backscatter coefficient (Mm^{-1}sr^{-1}) and the particle backscatter coefficient (β) profile (Mm^{-1}sr^{-1}, black vertical line) averaged between 18:00 and 21:00 (UTC), for the 20/10/2018 dust layer in Antikythera station. Areas of increased particle concentration are denoted with red tones, while the beta values reach up to 5 (Mm^{-1}sr^{-1}). The mean E-field appears enhanced and is consistently above the reference field showing an increase at ~21:00 (UTC), when dust deposition becomes prominent. Bottom panel: Volume Linear Depolarization Ratio (δ$_v$, %) for the same dust layer as obtained from the Polly^{XT} lidar and the Particle Linear Depolarization Ratio (δ$_p$, %) profile (black vertical line). High δ$_v$ values (>20%) are indicative of dust particle presence and δ$_p$ values between 25% - 30% in the afternoon are characteristic of pure dust.

Electric Field strength vs Attenuated Backscatter Coefficient at 532nm - March 16th 2018, Finokalia
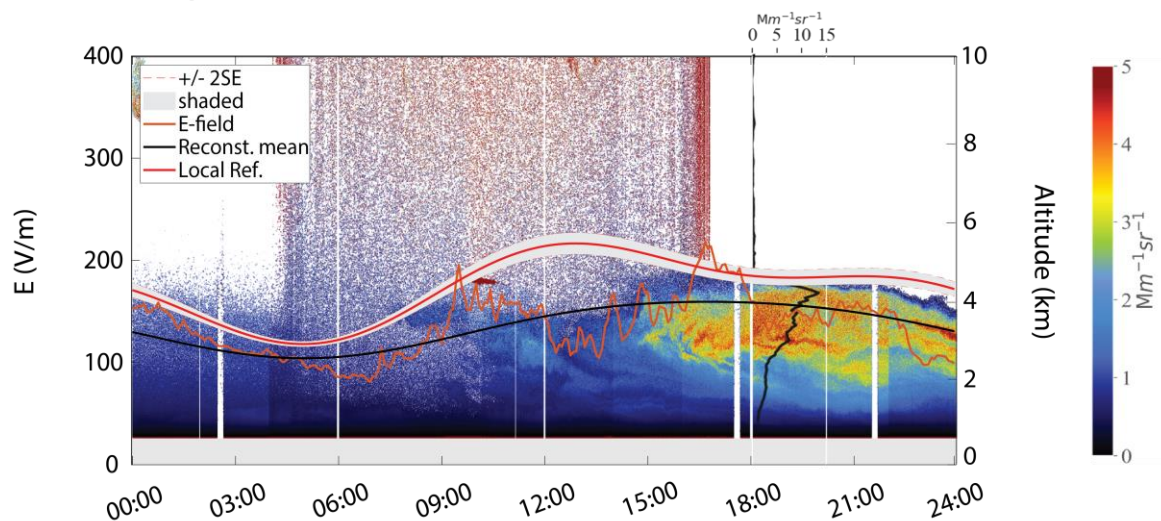
PollyXT Volume Linear Depolarization Ratio at 532nm - March 16th 2018, Finokalia

Time of Day (UTC)

810
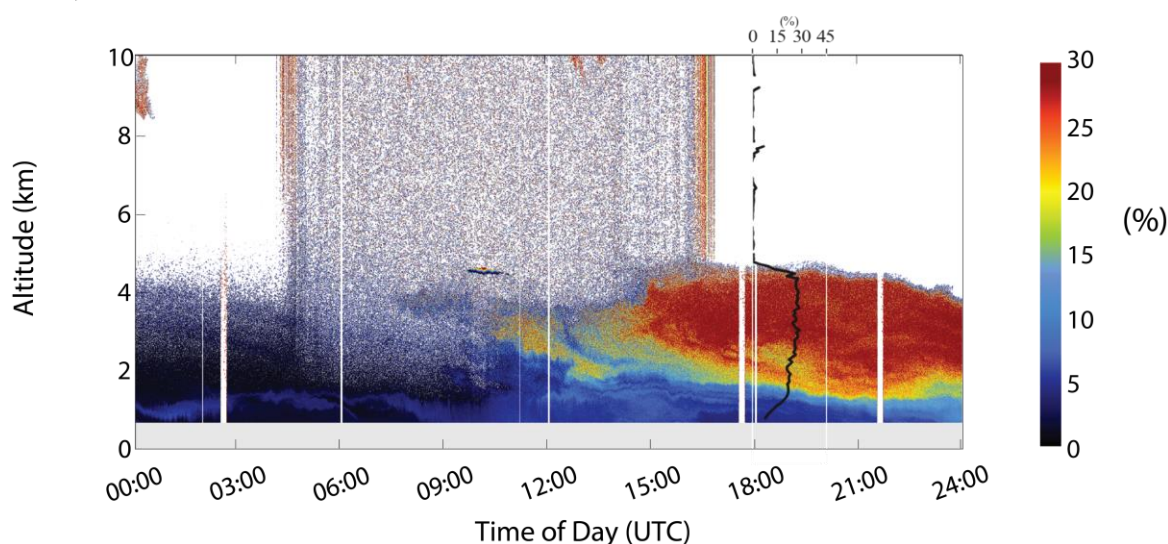
Fig. 8. Top panel: **Timeseries of the vertical electric field strength (orange), the Localized Reference Electric Field (red) and the reconstructed mean electric field variation (black) plotted with the time-height evolution of the attenuated backscatter coefficient (Mm⁻¹sr⁻¹) and the particle backscatter coefficient (β) profile (Mm⁻¹sr⁻¹, black vertical line) averaged between 18:00 and 21:00 (UTC), for the 16/03/2018 dust layer in Finokalia station. Areas of increased particle concentration are denoted with red tones, while the β values reach up to 15 (Mm⁻¹sr⁻¹). The mean E-field remains positive but well below the reference field, exhibiting an increase as particle injection initiates at ~11:00 (UTC) and then a decrease along the plume's progression.** Bottom panel: **Volume Linear Depolarization Ratio (VLDR, %) for the same dust layer as obtained from the PollyXT lidar and the Particle Linear Depolarization Ratio (PLDR, %) profile (black vertical line). VLDR values close to 30% are indicative of high dust particle concentration and PLDR values persistently of 30% are characteristic of pure dust within the entirety of the layer (1-4 km).**

Electric Field strength vs Attenuated Backscatter Coefficient at 532nm - June 23rd 2019, Antikythera
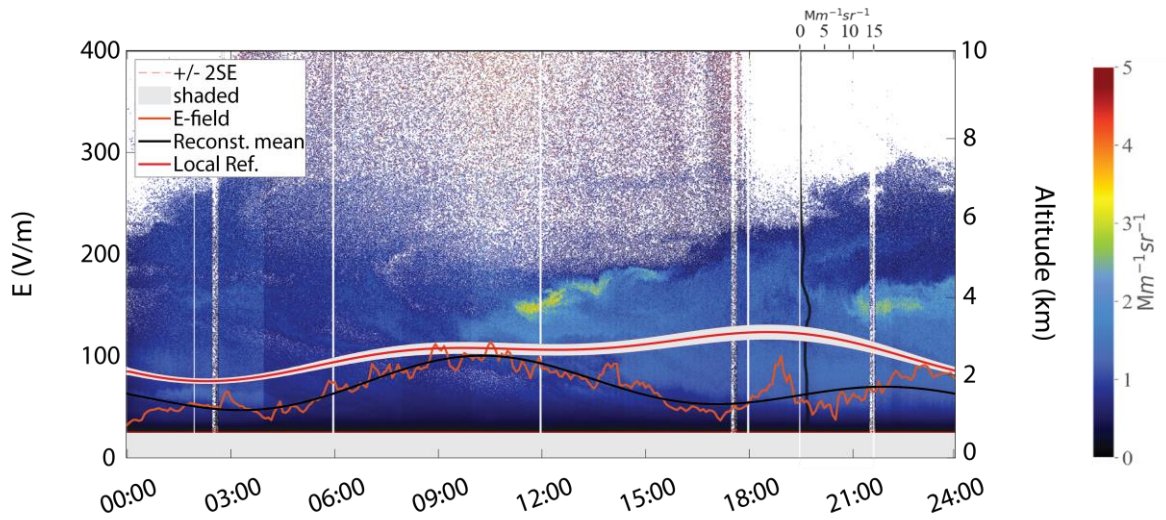
Polly^{XT} Volume Linear Depolarization Ratio at 532nm - June 23rd 2019, Antikythera
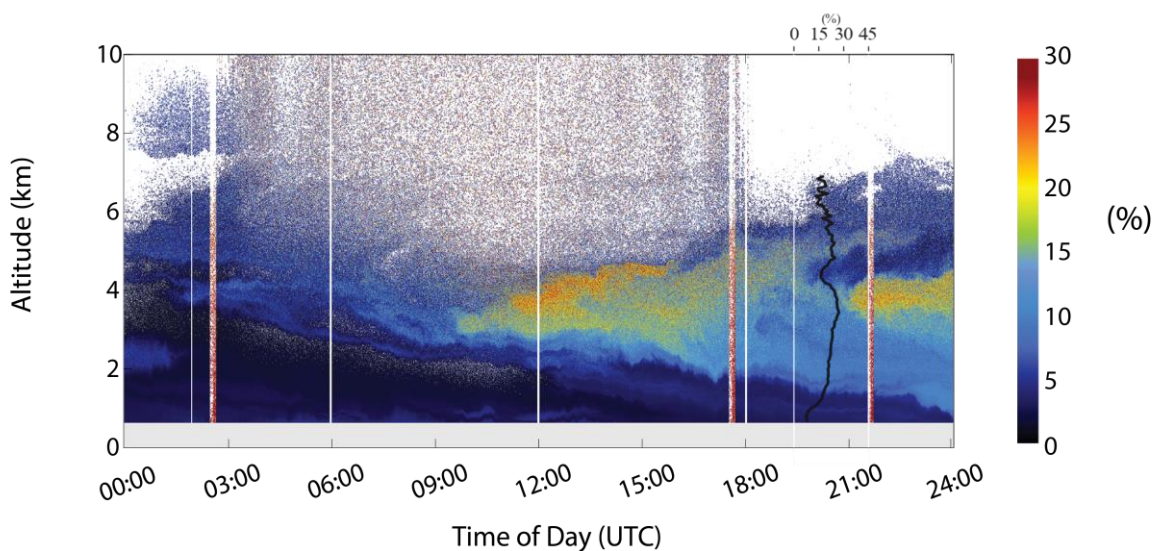
Fig. 9. Top panel**: Timeseries of the vertical electric field strength (orange), the Localized Reference Electric Field (red) and the reconstructed mean electric field variation (black) plotted with the time-height evolution of the attenuated backscatter coefficient (Mm^{-1}sr^{-1}) and the particle backscatter coefficient (β) profile (Mm^{-1}sr^{-1}, black vertical line) averaged between 18:00 and 21:00 (UTC), for the 23/06/2019 dust layer in Antikythera station. Areas of increased particle concentration are denoted with yellow to reddish tones, while the β values are between 3 to 4 (Mm^{-1}sr^{-1}). The mean E-field is positive and consistently below the reference field, exhibiting an increase when particle injection begins towards noon and further drops as the layer progresses to lower altitudes. Bottom panel: Volume Linear Depolarization Ratio (δ$_v$, %) for the same dust layer as obtained from the Polly^{XT} lidar and the Particle Linear Depolarization Ratio (δ$_p$, %) profile (black vertical line). High δ$_v$ values (>15%) are indicative of dust particle presence and δ$_p$ values between 25% - 30% in the afternoon are characteristic of pure dust.**
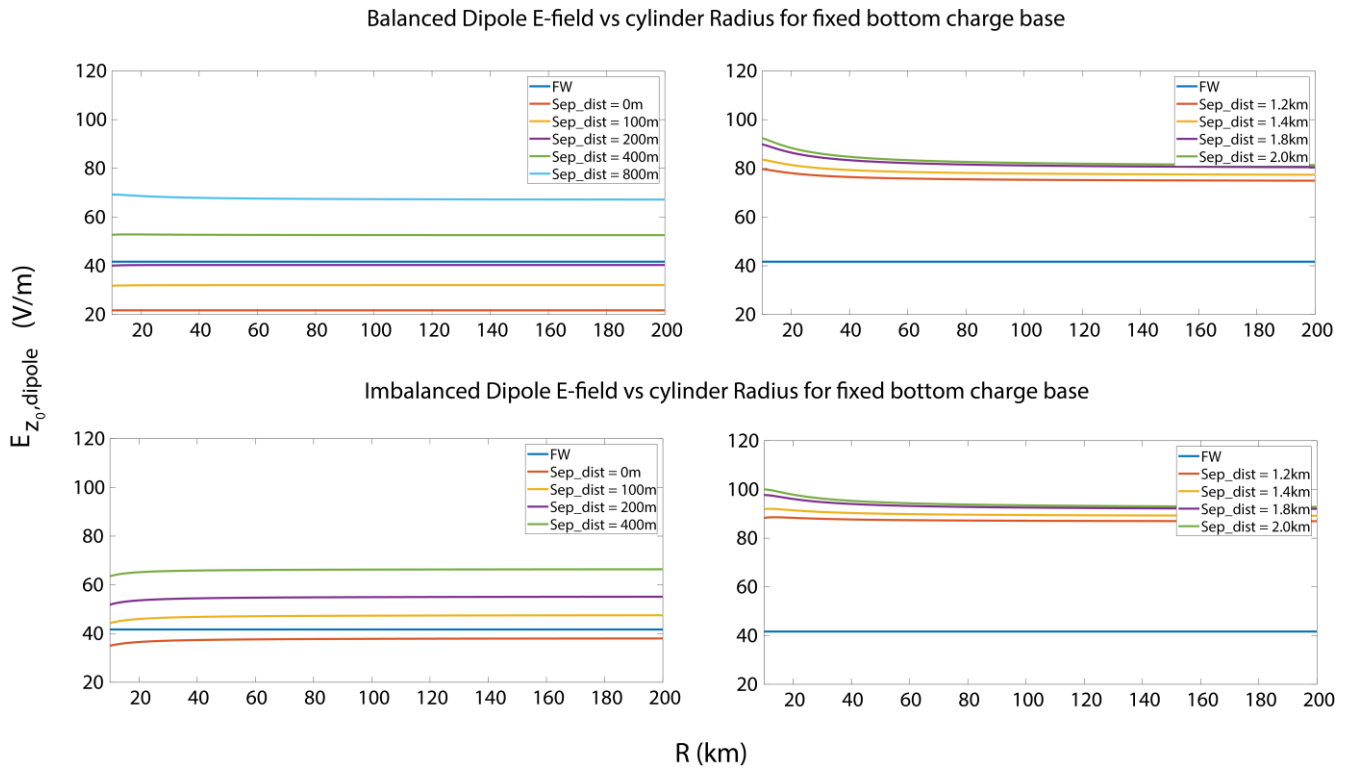
Fig. 10. Dipole electric field strength at ground level, $E_{z_0, dipole}$, as a function of the cylinder radius R, with the bottom cylinder at 2 km fixed central height within the dust layer. The separation distance between the upper and bottom charged layer increases as the upper cylinder moves towards the top of the dust layer, for both cases of balanced and imbalanced dipoles.
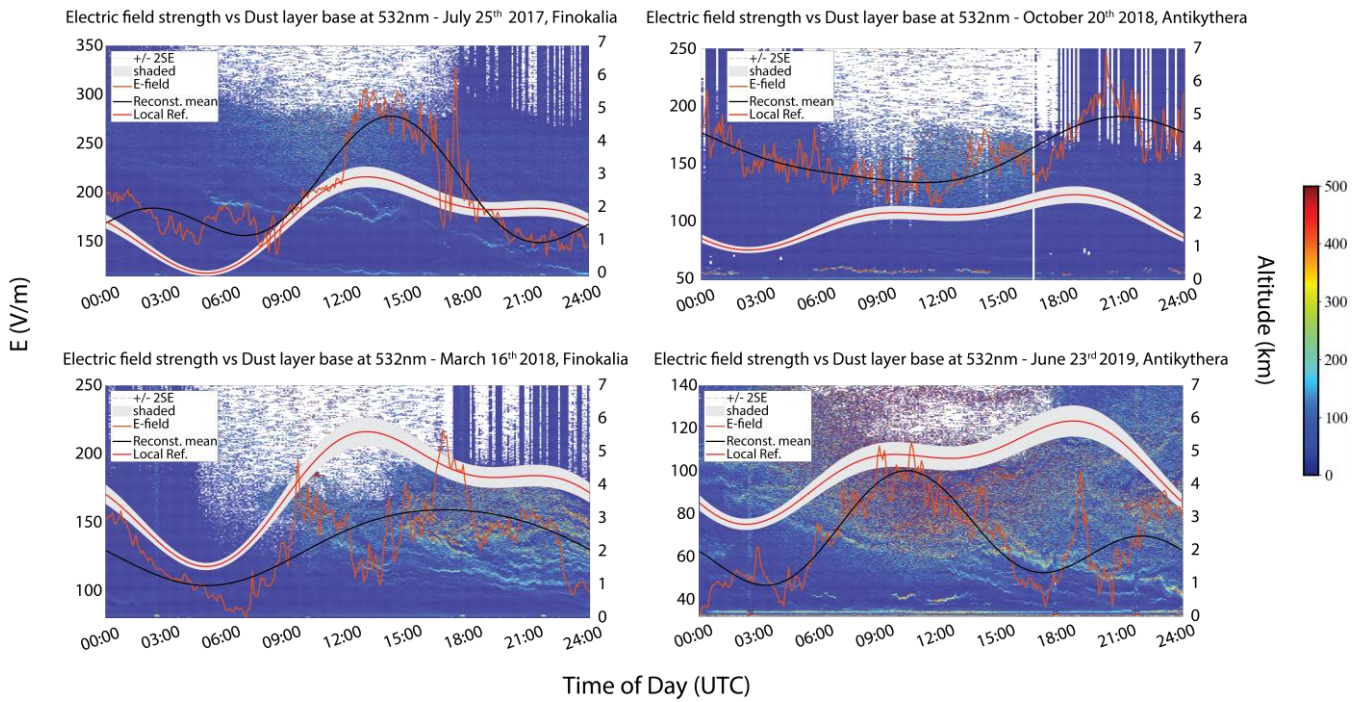
Fig. 11. Timeseries of the vertical electric field strength (orange), the Localized Reference Electric Field (red) and the reconstructed mean variation (black), plotted against the time-height evolution of the first derivative attenuated backscatter coefficient (cross component) at 532 nm, for the dust cases of 25/07/2017, 20/10/2018, 16/04/2018 and 23/06/2019. The dust layer bottom base is signified by the positive maximum values of the derivative within the 0-500 colorbar range.
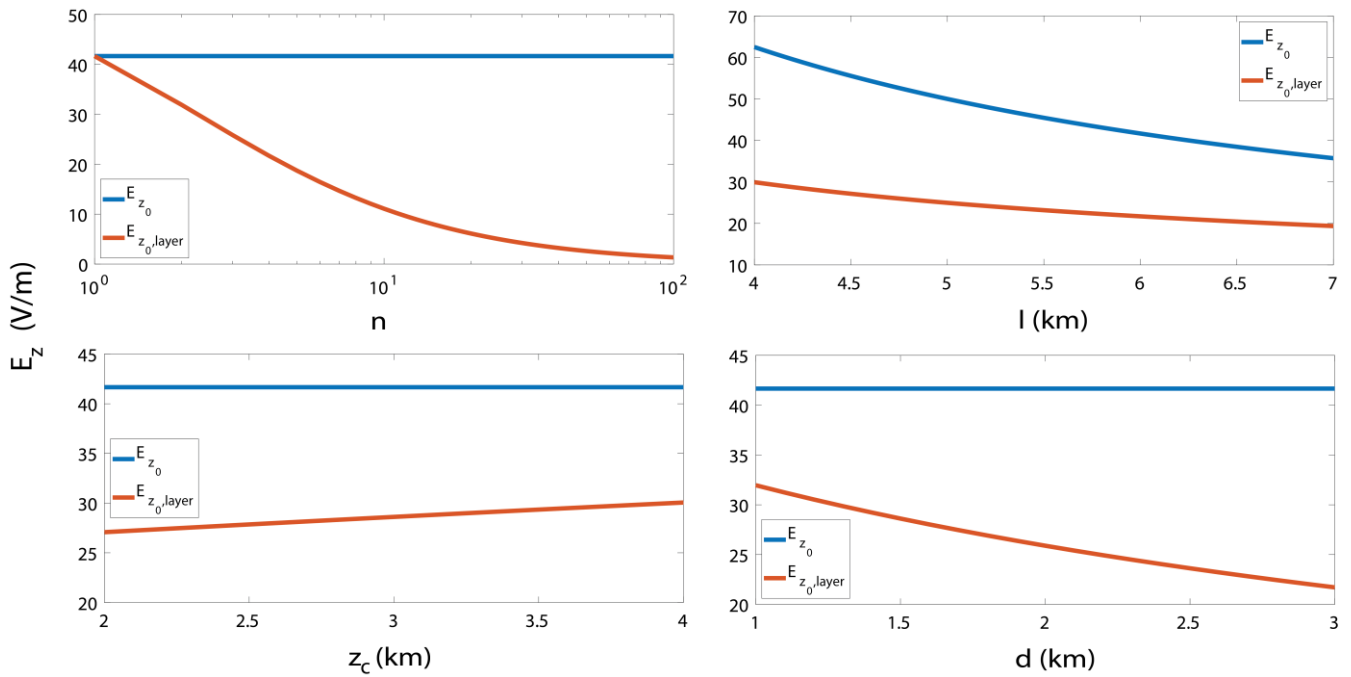
Fig. A1. Dependence of the vertical electric field, at ground level, under fair weather (E_{z_0}, blue line) and under the influence of an electrically neutral dust layer ($E_{z_0,layer}$, red line) on: (a) the reduction factor n, (b) the scaling height l, (c) the central layer height z_c and (d) the dust layer depth d, for $1/\sigma_0 = 3 \cdot 10^{13}$ Ω m, $V_{ion} = 250$ kV and H = 70 km. $E_{z_0,layer}$ strongly depends on the conductivity reduction as depicted in the case (a) curve, where the field reduces with the increasing reduction factor more effectively than with respect to the other three parameters. E_{z_0} depends only on the scaling height as expected.